

Data-driven quadratic modeling in the Loewner framework

D. S. Karachalios* I. V. Gosea[†] L. Gkimisis[†] A. C. Antoulas[‡]

*Max Planck Institute for Dynamics of Complex Technical Systems, Magdeburg, Germany and current affiliation: Institute for Electrical Engineering in Medicine, University of Luebeck, Germany.

Email: karachalios@mpi-magdeburg.mpg.de, ORCID: 0000-0001-9566-0076

[†]Max Planck Institute for Dynamics of Complex Technical Systems, Magdeburg, Germany.

Email: gosea@mpi-magdeburg.mpg.de, ORCID: 0000-0003-3580-4116

[†]Max Planck Institute for Dynamics of Complex Technical Systems, Magdeburg, Germany.

Email: gkimisis@mpi-magdeburg.mpg.de

[‡]Max Planck Institute for Dynamics of Complex Technical Systems, Magdeburg, Germany and Rice University, Electrical and Computer Engineering Department, Houston, TX 77005, USA and Baylor College of Medicine, Houston, TX 77030, USA.

Email: aca@rice.edu

Abstract: In this work, we present a non-intrusive, i.e., purely data-driven method that uses the Loewner framework (LF) along with nonlinear optimization techniques to identify or reduce quadratic control systems from input-output (i/o) time-domain measurements. At the heart of this method are optimization schemes that enforce interpolation of the symmetric generalized frequency response functions (GFRFs) as derived in the Volterra series framework. We consider harmonic input excitations to infer such measurements. After reaching the steady-state profile, the symmetric GFRFs can be measured from the Fourier spectrum (phase and amplitude). By properly using these measurements, we can identify low-order nonlinear state-space models with non-trivial equilibrium state points in the quadratic form, such as the Lorenz attractor. In particular, for the multi-point equilibrium case, where measurements describe some local bifurcated models to different coordinates, we achieve global model identification after solving an operator alignment problem based on a constrained quadratic matrix equation. We test the new method for a more demanding system in terms of state dimension, i.e., the viscous Burgers' equation with Robin boundary conditions. The complexity reduction and approximation accuracy are tested. Future directions and challenges conclude this work.

Keywords: data-driven methods, model reduction, system identification, Loewner framework, quadratic state-space modeling, Lorenz attractor, viscous Burgers' equation, Volterra series, quadratic matrix and vector equations.

AMS subject classifications: 93B15, 93C15, 93C10, 65F45

Novelty statement: The attributes of the proposed method can be summarized as:

- It constructs nonlinear (quadratic control) state-space models from input-output time domain data that serve the model reduction and identification aims.
- It achieves global identification of low-order quadratic control systems that can be bifurcated and measured only locally.
- It offers solution algorithms for 1) a quadratic vector equation that enforces higher order kernel interpolation (nonlinear optimization) and 2) a constrained quadratic matrix equation that aligns the resulting invariant operators after bifurcation.
- It is applied to various numerical examples, e.g., the Lorenz attractor and the viscous Burgers' equation, to illustrate the method's practical applicability.

1. Introduction

Mathematical modeling should be consistent with the physical laws when engineering applications are under consideration. Building surrogate models for robust simulation, design, and control is a worthwhile engineering task and methods that can interpret or discover governing equations [18] are essential and need to be reliable. Modeling with partial differential equations (PDEs) allow continuous descriptions of the physical variables, and numerically, discrete approximations of PDEs result in systems of ordinary differential equations (ODEs). Even with the recent development of high-performance computing (HPC) environments, the resulting dynamical models still inherit high complexity that must be handled carefully. Therefore approximation of large-scale dynamical systems [2] is pivotal for serving the scope of efficient simulation. The technique for reducing the complexity is known as model order reduction (MOR) [11–13]. There are many ways of reducing large-scale models, and each method is tailored to specific applications and goals for complexity reduction. A good distinction among methods has to do with the accessibility or not of a high-fidelity model (intrusive or non-intrusive). For the intrusive case where a model is available, methods such as balanced truncation (BT) (see the recent survey [17]) and moment matching (MM) (with the recent survey [8] and the references therein) for constructing surrogate models of low order that approximate the original without losing much accuracy, offering an error bound (BT), and with a guarantee on stability (BT and some MM variants) were extensively used. Additional MOR methods for nonlinear systems were also developed (basically, by extending the linear counterpart of BT, MM or others) [3, 7].

On the other hand, the ever-increasing availability of data, i.e., measurements related to the original model, initiate non-intrusive techniques such as Machine learning (ML) combined with model-based methods [18]. For specific tasks, e.g., pattern recognition, ML has demonstrated remarkable success. The limitations of ML methods arise when the interpretation of the derived models is under consideration. Therefore, model-based data assimilation through MOR techniques such as the proper orthogonal decomposition (POD)[53], the dynamic mode decomposition. (DMD)[31, 48, 50], the operator inference (OpInf) [10, 39, 47] have become popular. In many cases, there may not be an accurate description of the original model (the large-scale dynamical system) but only at specific measurements (snapshots in the time domain, spectrum description, etc.). Therefore, one of the main challenges is the reliability of the information extracted from the data. The mentioned data-driven methods (OpInf, DMD) and others, such as the sparse identification of dynamical systems (SINDY)[19] use state-access snapshot measurements to achieve model discovery that could be input dependent. Towards the same aim of model discovery without using state-access measurements and building input invariant models, the Loewner framework constitutes a non-intrusive method that deals directly with i/o data (real-world measurements used in most of the applied sciences, e.g., frequency, velocity, voltage, charge, or concentration) able to identify linear and nonlinear systems and simultaneously to offer the opportunity for complexity reduction. One way to reduce the model complexity is to employ interpolation. Out of the many available existing methods, we mention those based on rational approximation. Here, we mention the Loewner framework [44], the vector fitting (VF) [30] and the AAA algorithm [45]. We refer the reader to the extensive analysis provided in [3] for more details on such methods.

The realization of linear models is introduced in [32] and has been extended further in [34]. For the nonlinear case, extensions to the realization algorithm (i.e., by means of the subspace method) in the case of discrete-time bilinear control systems can be found in [20, 22, 33, 42] with the references within, and for linear parametric varying (LPV) systems in [51] when the scheduling signals can be measured. Other methods for data-driven system identification or reduction based on nonlinear autoregressive moving average with exogenous inputs (NARMAX) models can be found in [21] and in connection with Koopman operator and Wiener projection in [41]. Time discretization of semi-discretized in space nonlinear systems have disadvantages with the structure preservation for the resulting full-discretized model. A few schemes can preserve the structure, e.g., the forward Euler and for bilinear systems, but inherits conditional numerical stability, limiting the method to very short sampling times. On that account, a viable alternative is to devise methods that directly learn the continuous in-time operators without adding another discretization error due to the time mesh. The Fourier transform through the

classical Nyquist theorem provides a way to transform discrete information into perfect continuous signal reconstruction from a finite spectrum if the correct sampling frequency has been considered.

The LF is a non-intrusive interpolatory MOR technique that identifies state-space systems for certain generalized nonlinear classes, particularly: bilinear systems [5], linear switched systems [27], linear parameter-varying systems [28], quadratic-bilinear systems [4, 24, 25], and polynomial systems [9]. The aforementioned nonlinear variants of the Loewner framework construct efficient surrogate models from sampled data with direct numerical simulation (DNS) on the regular Volterra kernels derived from a prior accessible high-fidelity model. The challenging aspect of the regular multivariate Volterra kernels is that they cannot be inferred directly from a physical measurement setup when the underlying model is not accessible, and only a specific structure has been assumed (e.g., quadratic). Therefore, in a natural measurement environment (e.g., output in the time domain), the appropriate Volterra kernels that we can measure are of the symmetric type and can be derived with the growing exponential approach that is tailored to the probing method. The LF has been already extended to handle input-output data in the time domain for linear systems [46]. Similar studies towards the same goals for nonlinear can be found; bilinear [36]; quadratic-bilinear [26, 38].

Consequently, we are ready to introduce and analyze our new method that uses i/o time domain data to identify or construct quadratic state-space models after combining the Loewner and Volterra frameworks with nonlinear optimization techniques. Compared to our prior work [26, 36, 38], the advances are; 1) we use generalized frequency measurements from higher orders kernels of the symmetric type that explain the propagating harmonics in the time domain output (measurable), making the reverse process (from time to frequency) feasible through the Fourier transform; 2) we solve the resulting nonlinear optimization problems to achieve quadratic model construction that interpolates the Volterra series to more kernels; 3) we identify global quadratic systems of low order with nontrivial equilibrium points after measuring the local dynamical behavior and solving a nonlinear matrix equation; 4) we test the proposed method for both scopes of identification and reduction with classical benchmarks such as the forced Lorenz attractor and the viscous Burgers' equation. The rest of the paper is organized as follows; Section 2 presents the analyses and methods, starting from the linear case to the quadratic model construction. In many cases, the dynamics can be measured around non-zero equilibrium points. Therefore, analysis for such systems is included. Section 3, we illustrate different cases of identifying the forced Lorenz attractor with trivial and non-trivial equilibrium points. The method is also tested for the reduction/accuracy performance of the viscous Burgers' model. Section 4 summarizes the findings and future research directions.

2. Analysis and methods

We start with linear system theory providing explicit solutions and derivations of substantial quantities such as the transfer function. Next, we introduce the Loewner framework as an interpolatory tool in the linear case and explain how one can identify minimal linear systems from time domain measurements [46]. Continuously, approximation of nonlinear systems with the Volterra series is introduced with a focus on the quadratic state-space control system case. Analytical derivations of extracting the symmetric generalized frequency response functions with the probing method are presented. Further, the analysis of bifurcating quadratic systems is detailed by addressing the issue of local-equilibrium measurements and operator alignment. Finally, the chapter concludes with the proposed method supported with concise algorithms that summarize the computational techniques with ease of use.

2.1. The linear time-invariant system

We start our analysis with the linear time-invariant (LTI) system in the single-input single-output (SISO) form as

$$\begin{cases} \mathbf{E}\dot{\mathbf{x}}(t) = \mathbf{A}\mathbf{x}(t) + \mathbf{B}u(t), \\ y(t) = \mathbf{C}\mathbf{x}(t) + \mathbf{D}u(t), \mathbf{x}(0) = \mathbf{x}_0 = \mathbf{0}, t \geq 0, \end{cases} \quad (1)$$

where the state-dimension is n , and the operators are: $\mathbf{E}, \mathbf{A} \in \mathbb{R}^{n \times n}$, $\mathbf{B}, \mathbf{C}^T \in \mathbb{R}^{n \times 1}$, $\mathbf{D} \in \mathbb{R}$. Concentrating in the ordinary differential equation (1), with a non-singular (e.g., invertible) \mathbf{E} matrix, we have the following explicit solution

$$\begin{aligned}
 \dot{\mathbf{x}}(t) &= \mathbf{E}^{-1} \mathbf{A} \mathbf{x}(t) + \mathbf{E}^{-1} \mathbf{B} u(t) \Rightarrow \frac{d}{dt} \left[e^{-\mathbf{E}^{-1} \mathbf{A} t} \mathbf{x}(t) \right] = e^{-\mathbf{E}^{-1} \mathbf{A} t} \mathbf{E}^{-1} \mathbf{B} u(t) \Rightarrow \\
 &\int_0^t \frac{d}{d\tau} \left[e^{-\mathbf{E}^{-1} \mathbf{A} \tau} \mathbf{x}(\tau) \right] d\tau = \int_0^t e^{-\mathbf{E}^{-1} \mathbf{A} \tau} \mathbf{E}^{-1} \mathbf{B} u(\tau) d\tau \Rightarrow \\
 e^{-\mathbf{E}^{-1} \mathbf{A} t} \mathbf{x}(t) - e^{-\mathbf{E}^{-1} \mathbf{A} \cdot 0} \mathbf{x}(0) &= \int_0^t e^{-\mathbf{E}^{-1} \mathbf{A} \tau} \mathbf{E}^{-1} \mathbf{B} u(\tau) d\tau \Rightarrow \\
 \mathbf{x}(t) &= e^{\mathbf{E}^{-1} \mathbf{A} t} \mathbf{x}(0) + \int_0^t e^{\mathbf{E}^{-1} \mathbf{A} (t-\tau)} \mathbf{E}^{-1} \mathbf{B} u(\tau) d\tau \Rightarrow \text{(with } \sigma = t - \tau) \\
 y(t) &= \mathbf{C} e^{\mathbf{E}^{-1} \mathbf{A} t} \mathbf{x}_0 + \int_0^t \underbrace{\mathbf{C} e^{\mathbf{E}^{-1} \mathbf{A} \sigma} \mathbf{E}^{-1} \mathbf{B}}_{h_1(\sigma)} u(t - \sigma) d\sigma + \mathbf{D} u(t).
 \end{aligned} \tag{2}$$

The input-output solution of an LTI system with zero-initial conditions $\mathbf{x}_0 = \mathbf{0}$ and a zero feed-forward term $\mathbf{D} = 0$, results to the convolution integral $y(t) = \int_0^t h_1(\sigma) u(t - \sigma) d\sigma$. On the other hand, direct application of the Laplace transform $\mathcal{L}(\cdot)$ in(1) will give

$$\begin{cases} \mathcal{L}[\mathbf{E}\dot{\mathbf{x}}(t)] = \mathcal{L}[\mathbf{A}\mathbf{x}(t)] + \mathcal{L}[\mathbf{B}u(t)], \\ \mathcal{L}[y(t)] = \mathcal{L}[\mathbf{C}\mathbf{x}(t)] + \mathcal{L}[\mathbf{D}u(t)], \end{cases} \Rightarrow \begin{cases} s\mathbf{E}\mathbf{X}(s) - \mathbf{E}\mathbf{x}_0 = \mathbf{A}\mathbf{X}(s) + \mathbf{B}U(s), \\ \mathbf{Y}(s) = \mathbf{C}\mathbf{X}(s) + \mathbf{D}U(s). \end{cases} \tag{3}$$

Solving the algebraic equation (3) w.r.t $\mathbf{X}(s)$ and substituting to the output equation above, we conclude to

$$Y(s) = \mathbf{C} [(s\mathbf{E} - \mathbf{A})^{-1} \mathbf{B} + \mathbf{D}] U(s) \Rightarrow H_1(s) := \frac{Y(s)}{U(s)} = \mathbf{C} [(s\mathbf{E} - \mathbf{A})^{-1} \mathbf{B} + \mathbf{D}]. \tag{4}$$

For the case where $\mathbf{D} = 0$, the Laplace transform of the impulse response $h_1(\sigma)$, $\sigma \in \mathbb{R}_+$, is the transfer function $H(s)$, $s \in \mathbb{C}$. Since in the sequel, we will assume that \mathbf{E} is invertible, we will denote it as the identity matrix $\mathbf{E} = \mathbf{I}$. Later on, for a concise representation, it is convenient to define the resolvent as

$$\Phi(s) = (s\mathbf{I} - \mathbf{A})^{-1} \in \mathbb{C}^{n \times n}. \tag{5}$$

2.2. The Loewner framework for LTIs

We start with an account of the Loewner framework (LF) in the linear case [1, 6, 36]. The LF is an interpolatory method that seeks reduced models whose transfer function matches that of the original system at selected interpolation points. In the case of SISO systems, the following rational scalar interpolation problem is formulated. Consider as given the set of complex-valued data: $\{(s_k, f_k(s_k)) \in \mathbb{C} \times \mathbb{C} : k = 1, \dots, 2n\}$. We partition these data into two disjoint subsets:

$$\mathbf{S} = \underbrace{[s_1, \dots, s_n]}_{\mu} \underbrace{[s_{n+1}, \dots, s_{2n}]}_{\lambda}, \quad \mathbf{F} = \underbrace{[f_1, \dots, f_n]}_{\mathbf{V}} \underbrace{[f_{n+1}, \dots, f_{2n}]}_{\mathbf{W}},$$

where $\mu_i = s_i$, $\lambda_i = s_{n+i}$, $v_i = f_i$, $w_i = f_{n+i}$ for $i = 1, \dots, n$.

The objective is to find $H(s) \in \mathbb{C}$ such that:

$$H(\mu_i) = v_i, \quad i = 1, \dots, n, \quad \text{and} \quad H(\lambda_j) = w_j, \quad j = 1, \dots, n. \tag{6}$$

The left data set is denoted as: $\mathbf{M} = [\mu_1, \dots, \mu_n] \in \mathbb{C}^{1 \times n}$, $\mathbf{V} = [v_1, \dots, v_n]^T \in \mathbb{C}^{n \times 1}$, while the right data set as: $\mathbf{A} = [\lambda_1, \dots, \lambda_n]^T \in \mathbb{C}^{n \times 1}$, $\mathbf{W} = [w_1, \dots, w_n] \in \mathbb{C}^{1 \times n}$. Interpolation points are determined by the problem or are selected to achieve given model reduction goals.

2.2.1. The Loewner matrices

Given a row array of complex numbers (μ_j, v_j) , $j = 1, \dots, n$, and a column array, (λ_i, w_i) , $i = 1, \dots, n$, (with λ_i and the μ_j mutually distinct) the associated Loewner matrix \mathbb{L} and the shifted Loewner matrix \mathbb{L}_s are defined as:

$$\mathbb{L} = \begin{bmatrix} \frac{v_1 - w_1}{\mu_1 - \lambda_1} & \dots & \frac{v_1 - w_n}{\mu_1 - \lambda_n} \\ \vdots & \ddots & \vdots \\ \frac{v_n - w_1}{\mu_n - \lambda_1} & \dots & \frac{v_n - w_n}{\mu_n - \lambda_n} \end{bmatrix} \in \mathbb{C}^{n \times n}, \quad \mathbb{L}_s = \begin{bmatrix} \frac{\mu_1 v_1 - \lambda_1 w_1}{\mu_1 - \lambda_1} & \dots & \frac{\mu_1 v_1 - \lambda_n w_n}{\mu_1 - \lambda_n} \\ \vdots & \ddots & \vdots \\ \frac{\mu_n v_n - \lambda_1 w_1}{\mu_n - \lambda_1} & \dots & \frac{\mu_n v_n - \lambda_n w_n}{\mu_n - \lambda_n} \end{bmatrix} \in \mathbb{C}^{n \times n}.$$

Definition 2.1. If g is rational, i.e., $g(s) = \frac{p(s)}{q(s)}$, for appropriate polynomials p, q , the McMillan degree or the complexity of g is $\deg g = \max\{\deg(p), \deg(q)\}$.

Now, if $w_i = g(\lambda_i)$, and $v_j = g(\mu_j)$, are samples of a rational function g , the main property of Loewner matrices asserts the following.

Theorem 2.1. [1] Let \mathbb{L} be as above. If $k, q \geq \deg g$, then $\text{rank } \mathbb{L} = \deg g$. The rank of \mathbb{L} encodes the complexity of the underlying rational function g . Furthermore, the same result holds for matrix-valued functions g .

2.2.2. Construction of interpolants

If the pencil $(\mathbb{L}_s, \mathbb{L})$ is regular, then the quadruple $(\mathbf{E} = -\mathbb{L}, \mathbf{A} = -\mathbb{L}_s, \mathbf{B} = \mathbb{V}, \mathbf{C} = \mathbb{W})$, is a minimal realization of an interpolant for the data, i.e.,

$$H(s) = \mathbb{W}(\mathbb{L}_s - s\mathbb{L})^{-1}\mathbb{V}. \quad (7)$$

Otherwise, as shown in [1], the problem in (6) has a solution provided that

$$\text{rank } [s\mathbb{L} - \mathbb{L}_s] = \text{rank } [\mathbb{L}, \mathbb{L}_s] = \text{rank } \begin{bmatrix} \mathbb{L} & \mathbb{L}_s \end{bmatrix}^T = r,$$

for all $s \in \{\mu_i\} \cup \{\lambda_j\}$. Consider then the compact SVDs: $[\mathbb{L}, \mathbb{L}_s] = \mathbf{Y}\widehat{\Sigma}_r\tilde{\mathbf{X}}^*$, $\begin{bmatrix} \mathbb{L} & \mathbb{L}_s \end{bmatrix}^T = \tilde{\mathbf{Y}}\Sigma_r\mathbf{X}^*$, where $\widehat{\Sigma}_r, \Sigma_r \in \mathbb{R}^{r \times r}$, $\mathbf{Y} \in \mathbb{C}^{n \times r}$, $\mathbf{X} \in \mathbb{C}^{n \times r}$, $\tilde{\mathbf{Y}} \in \mathbb{C}^{2n \times r}$, $\tilde{\mathbf{X}} \in \mathbb{C}^{r \times 2n}$. The integer variable r can be chosen as the numerical rank (as opposed to the exact rank) of the Loewner pencil.

Theorem 2.2. The quadruple $(\tilde{\mathbf{A}}, \tilde{\mathbf{B}}, \tilde{\mathbf{C}}, \tilde{\mathbf{E}})$ of size $r \times r$, $r \times 1$, $1 \times r$, $r \times r$, given by:

$$\tilde{\mathbf{E}} = -\mathbf{Y}^T\mathbb{L}\mathbf{X}, \quad \tilde{\mathbf{A}} = -\mathbf{Y}^T\mathbb{L}_s\mathbf{X}, \quad \tilde{\mathbf{B}} = \mathbf{Y}^T\mathbb{V}, \quad \tilde{\mathbf{C}} = \mathbb{W}\mathbf{X},$$

is a descriptor realization of an (approximate) interpolant of the data with McMillan degree $r = \text{rank}(\mathbb{L})$, where

$$\tilde{H}(s) = \tilde{\mathbf{C}}(s\tilde{\mathbf{E}} - \tilde{\mathbf{A}})^{-1}\tilde{\mathbf{B}}. \quad (8)$$

For more details on the construction/identification of linear systems with the LF, we refer the reader to [3, 6, 36] where both the SISO and MIMO cases are addressed together with other more technical aspects (e.g., distribution of interpolation points, splitting of measurements, construction of real-valued models, etc.) and concise algorithms.

2.3. Nonlinear systems theory with the Volterra series representation

A wide class of nonlinear systems can be described by means of the Volterra-Wiener approach [14, 49]. In particular, the input-output relationship can be approximated by the Volterra series as

$$y(t) = \sum_{n=1}^N y_n(t), \quad y_n(t) = \int_{-\infty}^{\infty} \dots \int_{-\infty}^{\infty} h_n(\tau_1, \dots, \tau_n) \prod_{i=1}^n u(t - \tau_i) d\tau_i, \quad (9)$$

where $h_n(\tau_1, \dots, \tau_n)$ is a real-valued function of τ_1, \dots, τ_n known as the n th-order time-domain Volterra kernel. After a multivariate Laplace transform to the time-domain kernels $h_n(\tau_1, \dots, \tau_n)$, the n th-order generalized frequency response function (GFRF) is defined as

$$H_n(s_1, \dots, s_n) = \int_{-\infty}^{\infty} \dots \int_{-\infty}^{\infty} h_n(\tau_1, \dots, \tau_n) e^{\sum_{i=1}^n s_i \tau_i} d\tau_1 \dots d\tau_n. \quad (10)$$

The mathematical formulations above are for general nonlinear systems. Therefore, one way to derive specific kernels is to assume some structure of the underlying system that will explain the measurements due to some knowledge of physics, such as in the Navier-Stokes equation, where the dynamics are described from quadratic models. Further, many engineering examples that are driven with general analytical nonlinearities, after applying lifting techniques [23] can be represented with state polynomial nonlinearities into the lifted space and in the quadratic structure (11). As explained in [29], lifting strategies can result in polynomial systems of quadratic order in systems with ODEs or DAEs¹ where the non-invertible \mathbf{E} in the latter case makes the problem quite challenging even when state-access measurements (snapshots) can be accessed [39]; thus, we will not investigate such systems in this study with i/o data.

2.4. The quadratic system with control

We continue our analysis with the general state-space representation of a system in the quadratic form and for the SISO case:

$$\begin{cases} \dot{\mathbf{x}}(t) = \mathbf{A}\mathbf{x}(t) + \mathbf{Q}(\mathbf{x}(t) \otimes \mathbf{x}(t)) + \mathbf{B}u(t), \\ y(t) = \mathbf{C}\mathbf{x}(t), \quad \mathbf{x}(0) = \mathbf{x}_0 = \mathbf{0}, \quad t \geq 0, \end{cases} \quad (11)$$

where the state-dimension is n , and the operators are: $\mathbf{A} \in \mathbb{R}^{n \times n}$, $\mathbf{Q} \in \mathbb{R}^{n \times n^2}$, $\mathbf{B}, \mathbf{C}^T \in \mathbb{R}^{n \times 1}$. The Kronecker product \otimes is defined as in the following simple case $\begin{bmatrix} x_1 & x_2 \end{bmatrix} \otimes \begin{bmatrix} x_1 & x_2 \end{bmatrix} = \begin{bmatrix} x_1^2 & x_1 x_2 & x_2 x_1 & x_2^2 \end{bmatrix}$. Due to the commutative property, the matrix \mathbf{Q} denotes the Hessian of the right-hand side and exhibits a particular symmetric structure. For two arbitrary vectors $\mathbf{u}, \mathbf{v} \in \mathbb{R}^n$, we can always ensure that it holds

$$\mathbf{Q}(\mathbf{u} \otimes \mathbf{v}) = \mathbf{Q}(\mathbf{v} \otimes \mathbf{u}). \quad (12)$$

Similarly, we want representations of the underlying nonlinear system in both time and frequency domains as in the linear case. As we have exploited the tools such as the Volterra series expansion for approximating general nonlinear systems, we now focus on enforcing the structure of the quadratic state-space model. The first aim is to derive the symmetric GFRFs for the quadratic case that can be processed from the time domain to the frequency domain, and the second is to use these measurements to identify the hidden operators (\mathbf{A} , \mathbf{Q} , \mathbf{B} , \mathbf{C}).

2.4.1. Deriving higher-order transfer functions for the quadratic control system

The Volterra series (9) describes the approximation of nonlinear systems through higher-order generalized kernels in a multi-convolutional scheme. As explained in [49], different ways of extracting different kernels exist. One way is the variational approach, where the structure of the triangular (or regular kernels) can be revealed through Picard iterations. In particular, the regular kernels can be derived after shifting the frequency domain of the triangular kernels. The regular kernels are convenient due to the asymmetric structure that makes them valuable for interpolation frameworks such as the Loewner and its nonlinear extensions. Despite the intrusive ease of use, the regular Volterra kernels cannot be measured directly from the time domain. Therefore, we choose another way of deriving higher-order Volterra kernels, namely the growing exponential approach (e.g., the probing method) for treating the issue of kernel estimation. With probing (harmonic excitation) of the system, and after processing the

¹DAEs: Differential algebraic equations

steady-state time evolution in the frequency domain via the Fourier (special case of Laplace over the imaginary axis) transform, the time domain signal is decomposed to harmonics that scale and shift w.r.t. the symmetric GFRFs. Methods for estimating these symmetric kernels (e.g., kernel separation) were introduced in [16, 35, 52].

The Probing method. It was shown by Rugh [49] and Billings [14] that for nonlinear systems which are described by the Volterra model (9) and excited by a combination of complex exponentials $u(t) = \sum_{i=1}^R e^{s_i t}$, $1 \leq R \leq N$, the output response can be written as

$$\begin{aligned} y(t) &= \sum_{n=1}^N \sum_{i_1=1}^R \cdots \sum_{i_n=1}^R H_n(s_{i_1}, \dots, s_{i_n}) e^{(s_{i_1} + \cdots + s_{i_n})t}, \\ &= \sum_{n=1}^N \sum_{m(n)} \tilde{H}_{m_1(n) \dots m_R(n)}(s_1, \dots, s_R) e^{(m_1(n)s_1 + \cdots + m_R(n)s_R)t}, \end{aligned} \quad (13)$$

where $\sum_{m(n)}$ indicates an R -fold sum over all integer indices $m_1(n), \dots, m_R(n)$ such that $0 \leq m_i(n) \leq n$, $m_1(n) + \cdots + m_R(n) = n$, and

$$\tilde{H}_{m_1(n) \dots m_R(n)}(s_1, \dots, s_R) = \frac{n!}{m_1(n)! \cdots m_R(n)!} H_n(\underbrace{s_1, \dots, s_1}_{m_1(n)}, \dots, \underbrace{s_R, \dots, s_R}_{m_R(n)}). \quad (14)$$

Note that, \tilde{H}_n is the weighted GFRF, corresponding to H_n ; The former scales with the factor $\frac{n!}{m_1(n)! \cdots m_R(n)!}$. Note also that different input amplitudes can be considered as in [14, 54] where amplitude shifting allows kernel separation.

To determine the R th-order generalized frequency response function $H_R(s_1, \dots, s_R)$, the probing input $u(t) = \sum_{i=1}^R e^{s_i t}$ needs to be applied, with at least R harmonics. To simplify the next derivations, we introduce the input-state GFRFs $\mathbf{G}_i(s_1, \dots, s_i)$, $i = 1, \dots, n$. These simply result in the input-output GFRFs by multiplying the \mathbf{H}_i 's from the left with the output vector \mathbf{C} (in the SISO case), i.e., $H_n(s_1, \dots, s_n) = \mathbf{C} \mathbf{G}_n(s_1, \dots, s_n)$. Note further that the transfer function \mathbf{G}_i is a vector of length equal to the state dimension n (this latter is identical to \mathbf{H}_i , when $\mathbf{C} = \mathbf{I}_n$, i.e., when all the state elements are individually observed).

• **$R = 1$ - 1st order GFRF $H_1(s_1)$:** With input $u(t) = e^{s_1 t}$ the state solution $\mathbf{x}(t)$ and the time derivative $\dot{\mathbf{x}}(t)$ are respectively:

$$\mathbf{x}(t) = \sum_{n=1}^N \sum_{m(n)} \tilde{\mathbf{G}}_{m_1(n)}(s_1) e^{(m_1(n)s_1)t}, \quad \dot{\mathbf{x}}(t) = \sum_{n=1}^N \sum_{m(n)} \tilde{\mathbf{G}}_{m_1(n)}(s_1) m_1(n) s_1 e^{(m_1(n)s_1)t} \quad (15)$$

By substituting to the differential equation of the system (11), we have

$$\begin{aligned} \dot{\mathbf{x}}(t) - \mathbf{A} \mathbf{x}(t) - \mathbf{B} u(t) &= \sum_{n=1}^N \sum_{m(n)} (m_1(n) s_1 \mathbf{I} - \mathbf{A}) \tilde{\mathbf{G}}_{m_1(n)}(s_1) e^{(m_1(n)s_1)t} - \mathbf{B} e^{s_1 t} \\ &= \mathbf{Q} \left(\sum_{n=1}^N \sum_{m(n)} \tilde{\mathbf{G}}_{m_1(n)}(s_1) e^{(m_1(n)s_1)t} \otimes \sum_{n=1}^N \sum_{m(n)} \tilde{\mathbf{G}}_{m_1(n)}(s_1) e^{(m_1(n)s_1)t} \right). \end{aligned} \quad (16)$$

By collecting the terms with $e^{s_1 t}$, we result to

$$(s_1 \mathbf{I} - \mathbf{A}) \tilde{\mathbf{G}}_1(s_1) = \mathbf{B} \Rightarrow \tilde{\mathbf{G}}_1(s_1) = (s_1 \mathbf{I} - \mathbf{A})^{-1} \mathbf{B}. \quad (17)$$

We adjust in a similar way as in H_n the weighted $\mathbf{G}_1(s_1) = \frac{1!}{m_1(1)!} \tilde{\mathbf{G}}_1(s_1) = (s_1 \mathbf{I} - \mathbf{A})^{-1} \mathbf{B}$. Multiplication with the vector \mathbf{C} from the left gives the 1st order GFRF that is consistent with the linear subsystem and can be simplified further using the resolvent notation.

$$H_1(s_1) = \mathbf{C} (s_1 \mathbf{I} - \mathbf{A})^{-1} \mathbf{B} = \underbrace{\mathbf{C} \Phi(s_1)}_{\mathbf{G}_1(s_1)} \overbrace{\mathbf{B}}^{\mathbf{R}_1}. \quad (18)$$

Higher order kernels, e.g., H_2, H_3, \dots , can be derived at this level. Still, these can be evaluated only on the diagonal of the hyper-plane that span the domain of definition, e.g., $H_2(s_1, s_1)$, $H_3(s_1, s_1, s_1)$ which is not enough for achieving the identification goal as H_2 has a 2D domain support where a single harmonic input will always give information on the univariate diagonal (NFR method). Therefore, the next step is to excite with more complex inputs in terms of harmonics to identify the structure of the higher kernels.

- **$R = 2$ - 2nd order GFRF $H_2(s_1, s_2)$** : With input $u(t) = e^{s_1 t} + e^{s_2 t}$ the state solution is:

$$\mathbf{x}(t) = \sum_{n=1}^N \sum_{m(n)} \tilde{\mathbf{G}}_{m_1(n)m_2(n)}(s_1, s_2) e^{(m_1(n)s_1 + m_2(n)s_2)t}, \quad (19)$$

and the time derivative results to

$$\dot{\mathbf{x}}(t) = \sum_{n=1}^N \sum_{m(n)} (m_1(n)s_1 + m_2(n)s_2) \tilde{\mathbf{G}}_{m_1(n)m_2(n)}(s_1, s_2) e^{(m_1(n)s_1 + m_2(n)s_2)t}. \quad (20)$$

By substituting into the differential equation of the system (11), we obtain

$$\begin{aligned} \dot{\mathbf{x}}(t) - \mathbf{A}\mathbf{x}(t) &= \\ &= \sum_{n=1}^N \sum_{m(n)} ((m_1(n)s_1 + m_2(n)s_2)\mathbf{I} - \mathbf{A}) \tilde{\mathbf{G}}_{m_1(n)m_2(n)}(s_1, s_2) e^{(m_1(n)s_1 + m_2(n)s_2)t} \\ &= \mathbf{Q} \left(\sum_{n=1}^N \sum_{m(n)} \tilde{\mathbf{G}}_{m_1(n)m_2(n)}(s_1, s_2) e^{(m_1(n)s_1 + m_2(n)s_2)t} \otimes \dots \right. \\ &\quad \left. \dots \otimes \sum_{n=1}^N \sum_{m(n)} \tilde{\mathbf{G}}_{m_1(n)m_2(n)}(s_1, s_2) e^{(m_1(n)s_1 + m_2(n)s_2)t} \right) + \mathbf{B}(e^{s_1 t} + e^{s_2 t}). \end{aligned} \quad (21)$$

By collecting the terms $e^{s_1 t + s_2 t}$ with $(n = 2, m_1(2) = 1, m_2(2) = 1)$, we result to

$$\begin{aligned} &((s_1 + s_2)\mathbf{I} - \mathbf{A}) \tilde{\mathbf{G}}_{11}(s_1, s_2) e^{(s_1 + s_2)t} = \\ &= \mathbf{Q} \left[\tilde{\mathbf{G}}_{10}(s_1) e^{s_1 t} \otimes \tilde{\mathbf{G}}_{01}(s_2) e^{s_2 t} + \tilde{\mathbf{G}}_{01}(s_2) e^{s_2 t} \otimes \tilde{\mathbf{G}}_{10}(s_1) e^{s_1 t} \right] \Rightarrow \\ &((s_1 + s_2)\mathbf{I} - \mathbf{A}) \tilde{\mathbf{G}}_{11}(s_1, s_2) = \mathbf{Q} \left[\tilde{\mathbf{G}}_{10}(s_1) \otimes \tilde{\mathbf{G}}_{01}(s_2) + \tilde{\mathbf{G}}_{01}(s_2) \otimes \tilde{\mathbf{G}}_{10}(s_1) \right] \Rightarrow \\ &\tilde{\mathbf{G}}_{11}(s_1, s_2) = ((s_1 + s_2)\mathbf{I} - \mathbf{A})^{-1} \cdot \\ &\cdot \mathbf{Q} \left[(s_1\mathbf{I} - \mathbf{A})^{-1} \mathbf{B} \otimes (s_2\mathbf{I} - \mathbf{A})^{-1} \mathbf{B} + (s_2\mathbf{I} - \mathbf{A})^{-1} \mathbf{B} \otimes (s_1\mathbf{I} - \mathbf{A})^{-1} \mathbf{B} \right] \end{aligned} \quad (22)$$

Finally, by adjusting the weighted $\tilde{\mathbf{G}}_{11}(s_1, s_2) = \frac{2!}{1!1!} \mathbf{G}_2(s_1, s_2) = 2\mathbf{G}_2(s_1, s_2)$, and multiplying from the left with \mathbf{C} , we can define the 2nd order GFRF after using the resolvent notation as

$$\begin{aligned} H_2(s_1, s_2) &= \frac{1}{2} \mathbf{C} \Phi(s_1 + s_2) \mathbf{Q} \underbrace{[\Phi(s_1)\mathbf{B} \otimes \Phi(s_2)\mathbf{B} + \Phi(s_2)\mathbf{B} \otimes \Phi(s_1)\mathbf{B}]}_{\mathbf{R}_2(s_1, s_2)} \\ &= \mathbf{C} \frac{1}{2} \Phi(s_1 + s_2) \mathbf{Q} \underbrace{[\mathbf{G}_1(s_1) \otimes \mathbf{G}_1(s_2) + \mathbf{G}_1(s_2) \otimes \mathbf{G}_1(s_1)]}_{\mathbf{G}_2(s_1, s_2)} \end{aligned} \quad (23)$$

- **$R = 3$ - 3rd order GFRF $H_3(s_1, s_2, s_3)$** : With input $u(t) = e^{s_1 t} + e^{s_2 t} + e^{s_3 t}$, and similar argu-

ments, we can derive

$$\begin{aligned}
 H_3(s_1, s_2, s_3) &= \mathbf{C} \underbrace{\frac{1}{6} \Phi(s_1 + s_2 + s_3) \mathbf{Q} \mathbf{R}_3(s_1, s_2, s_3)}_{\mathbf{G}_3(s_1, s_2, s_3)}, \text{ with} \\
 \mathbf{R}_3(s_1, s_2, s_3) &= \mathbf{G}_1(s_1) \otimes \mathbf{G}_2(s_2, s_3) + \mathbf{G}_2(s_2, s_3) \otimes \mathbf{G}_1(s_1) + \\
 &\quad \mathbf{G}_1(s_2) \otimes \mathbf{G}_2(s_1, s_3) + \mathbf{G}_2(s_1, s_3) \otimes \mathbf{G}_1(s_2) + \\
 &\quad \mathbf{G}_1(s_3) \otimes \mathbf{G}_2(s_1, s_2) + \mathbf{G}_2(s_1, s_2) \otimes \mathbf{G}_1(s_3).
 \end{aligned} \tag{24}$$

At this point, we illustrate some of the properties the derived symmetric transfer functions inherit for the quadratic control system case.

- **Symmetry:** As it is evident, any permutation of the set (s_1, s_2, \dots, s_n) will result to the same evaluation of the $H_n(s_1, s_2, \dots, s_n)$ and $\mathbf{G}_n(s_1, s_2, \dots, s_n)$.
- **Decompositions:** Introducing the general reachability \mathcal{R} and observability \mathcal{O} counterparts, a more concise representation of the kernels can be achieved. As we have introduced the reachability matrices $\mathbf{R}_1, \mathbf{R}_2, \mathbf{R}_3$, here are the corresponding observability matrices:

$$\begin{aligned}
 \mathbf{O}_1(s_1) &= \mathbf{C} \Phi(s_1), \\
 \mathbf{O}_2(s_1, s_2) &= \frac{1}{2} \mathbf{C} \Phi(s_1 + s_2), \\
 \mathbf{O}_3(s_1, s_2, s_3) &= \frac{1}{6} \mathbf{C} \Phi(s_1 + s_2 + s_3).
 \end{aligned} \tag{25}$$

Next, we introduce the following [table 1](#) that illustrates the dependencies of the quadratic operator as these are decomposed in observability and reachability counterparts. With the above

input-output GFRF	\mathcal{O}	\mathcal{R}
$H_1(s_1)$	$\mathbf{O}_1(s_1)$	$\mathbf{R}_1 = \mathbf{B}$
$H_2(s_1, s_2, \mathbf{Q})$	$\mathbf{O}_2(s_1, s_2)$	$\mathbf{R}_2(s_1, s_2)$
$H_3(s_1, s_2, s_3, \mathbf{Q})$	$\mathbf{O}_3(s_1, s_2, s_3)$	$\mathbf{R}_3(s_1, s_2, s_3, \mathbf{Q})$

Table 1: Quadratic operator dependency over the input to state kernels with respect to the generalized controllability and observability counterparts.

observations and notations, we can derive a more convenient representation of the input to state GFRFs by exploiting their structure and stressing the positioning of the quadratic operator as in the 3rd level with the superscripts $(\cdot)^\ell$ -left and $(\cdot)^r$ -right.

$$\begin{aligned}
 \mathbf{G}_1(s_1) &= \Phi(s_1) \mathbf{R}_1, \\
 \mathbf{G}_2(s_1, s_2, \mathbf{Q}) &= \frac{1}{2} \Phi(s_1, s_2) \mathbf{Q} \mathbf{R}_2(s_1, s_2), \\
 \mathbf{G}_3(s_1, s_2, s_3, \mathbf{Q}^\ell, \mathbf{Q}^r) &= \frac{1}{6} \Phi(s_1, s_2, s_3) \mathbf{Q}^\ell \mathbf{R}_3(s_1, s_2, s_3, \mathbf{Q}^r)
 \end{aligned} \tag{26}$$

and for the input to output GFRFs as

$$\begin{aligned}
 H_1(s_1) &= \mathbf{O}_1(s_1) \mathbf{R}_1, \\
 H_2(s_1, s_2, \mathbf{Q}) &= \mathbf{O}_2(s_1, s_2) \mathbf{Q} \mathbf{R}_2(s_1, s_2), \\
 H_3^{\ell r}(s_1, s_2, s_3, \mathbf{Q}^\ell, \mathbf{Q}^r) &= \mathbf{O}_3(s_1, s_2, s_3) \mathbf{Q}^\ell \mathbf{R}_3(s_1, s_2, s_3, \mathbf{Q}^r).
 \end{aligned} \tag{27}$$

- **The reachability matrix $\mathbf{R}_3(\mathbf{Q})$ is linear w.r.t the quadratic operator \mathbf{Q} .** Assume $\lambda_1, \lambda_2 \in \mathbb{R}$ and $\mathbf{Q}_1, \mathbf{Q}_2 \in \mathbb{R}^{n \times n^2}$. Then, it holds

– **Linear property:** $\mathbf{R}_3(\lambda_1 \mathbf{Q}_1 + \lambda_2 \mathbf{Q}_2) = \lambda_1 \mathbf{R}_3(\mathbf{Q}_1) + \lambda_2 \mathbf{R}_3(\mathbf{Q}_2)$.

Proof. By neglecting the similar-structured terms (s.s.t), we can prove the following:

$$\begin{aligned}
\mathbf{R}_3(s_1, s_2, s_3, \lambda_1 \mathbf{Q}_1 + \lambda_2 \mathbf{Q}_2) &= \mathbf{G}_1(s_1) \otimes \mathbf{G}_2(s_2, s_3, \lambda_1 \mathbf{Q}_1 + \lambda_2 \mathbf{Q}_2) + s.s.t. \\
&= \mathbf{G}_1(s_1) \otimes \frac{1}{2} \Phi(s_1, s_2) (\lambda_1 \mathbf{Q}_1 + \lambda_2 \mathbf{Q}_2) \mathbf{R}_2(s_1, s_2) + s.s.t. \\
&= \mathbf{G}_1(s_1) \otimes \frac{1}{2} \Phi(s_1, s_2) \lambda_1 \mathbf{Q}_1 \mathbf{R}_2(s_1, s_2) + \mathbf{G}_1(s_1) \otimes \frac{1}{2} \Phi(s_1, s_2) \lambda_2 \mathbf{Q}_2 \mathbf{R}_2(s_1, s_2) + s.s.t. \\
&= \lambda_1 \mathbf{G}_1(s_1) \otimes \mathbf{G}_2(s_2, s_3, \mathbf{Q}_1) + \lambda_2 \mathbf{G}_1(s_1) \otimes \mathbf{G}_2(s_2, s_3, \mathbf{Q}_2) + s.s.t. \\
&= \lambda_1 \mathbf{R}_3(s_1, s_2, s_3, \mathbf{Q}_1) + \lambda_2 \mathbf{R}_3(s_1, s_2, s_3, \mathbf{Q}_2).
\end{aligned}$$

□

Starting from the original dynamical system in (11) with the quadratic nonlinearity, we have derived all the quantities of interest with their properties for setting up our method. Equivalent descriptions between the time and frequency domain representations have been addressed for this problem using the Volterra theory.

2.5. Method for quadratic modeling from i/o time domain data

Next, we introduce the proposed method for computing quadratic state-space models from the first three symmetric GFRFs, which can be measured from time-domain harmonic excitation.

2.5.1. Identification of the linear subsystem with the Loewner framework

Using measurements of the 1st harmonic, we can identify the minimal linear subsystem of order $r \leq n$, with an invertible $\hat{\mathbf{E}}$ as $(\hat{\mathbf{A}}, \hat{\mathbf{B}}, \hat{\mathbf{C}})$ with the Loewner framework. Further, by having access to the identified linear subsystem, we can formulate optimization problems where estimations of the quadratic operator can be achieved after using information from the higher harmonics (kernels). We acquire and solve these optimization problems in two steps; first, by solving an under-determined linear optimization problem in a least-squares setting, and second, by solving a non-linear optimization problem with the Newton method.

2.5.2. Estimation of the quadratic operator from the 2nd kernel

Identification of the minimal linear subsystem $(\hat{\mathbf{A}}, \hat{\mathbf{B}}, \hat{\mathbf{C}})$ of order r as described in section 2.5.1 allows the construction of the reduced resolvent $\hat{\Phi}(s) = (s\hat{\mathbf{I}} - \hat{\mathbf{A}})^{-1} \in \mathbb{C}^{r \times r}$, and the 2nd GFRFs with the unknown operator $\hat{\mathbf{Q}}$ can be written as:

$$\begin{aligned}
\hat{H}_2(s_1, s_2) &= \underbrace{\frac{1}{2} \hat{\mathbf{C}} \hat{\Phi}(s_1 + s_2)}_{\hat{\mathbf{O}}_2(s_1, s_2)} \underbrace{\hat{\mathbf{Q}} \left[\hat{\Phi}(s_1) \hat{\mathbf{B}} \otimes \hat{\Phi}(s_2) \hat{\mathbf{B}} + \hat{\Phi}(s_2) \hat{\mathbf{B}} \otimes \hat{\Phi}(s_1) \hat{\mathbf{B}} \right]}_{\hat{\mathbf{R}}_2(s_1, s_2)} \\
&= \hat{\mathbf{O}}_2(s_1, s_2) \hat{\mathbf{Q}} \hat{\mathbf{R}}_2(s_1, s_2) = \left(\hat{\mathbf{O}}_2(s_1, s_2) \otimes \hat{\mathbf{R}}_2^T(s_1, s_2) \right) \text{vec}(\hat{\mathbf{Q}}).
\end{aligned} \tag{28}$$

The way of estimating the quadratic operator $\hat{\mathbf{Q}}$ comes after enforcing interpolation with the 2nd harmonic (2nd kernel) over a 2D grid of selected measurements $(s_1^{(k)}, s_2^{(k)})$. Thus, we enforce

$$\underbrace{H_2(s_1^{(k)}, s_2^{(k)})}_{\text{k: measurements}} = \hat{H}_2(s_1^{(k)}, s_2^{(k)}), \tag{29}$$

and we construct the following linear optimization problem that is solvable by minimizing the 2-norm (least-squares) in a similar way as in the quadratic-bilinear case in [38]. Collecting k pairs of measurements $(s_1^{(k)}, s_2^{(k)})$, we conclude to:

$$\underbrace{\begin{bmatrix} H_2(s_1^{(1)}, s_2^{(1)}) \\ H_2(s_1^{(2)}, s_2^{(2)}) \\ \vdots \\ H_2(s_1^{(k)}, s_2^{(k)}) \end{bmatrix}}_{\mathbf{Y}: (k \times 1)} = \underbrace{\begin{bmatrix} \hat{\mathbf{O}}_2^{(1)} \otimes \hat{\mathbf{R}}_2^{T(1)} \\ \hat{\mathbf{O}}_2^{(2)} \otimes \hat{\mathbf{R}}_2^{T(2)} \\ \vdots \\ \hat{\mathbf{O}}_2^{(k)} \otimes \hat{\mathbf{R}}_2^{T(k)} \end{bmatrix}}_{\mathbf{M}: (k \times r^3)} \underbrace{\text{vec}(\hat{\mathbf{Q}})}_{r^3 \times 1} \quad (30)$$

The quadratic operator inherits symmetries, e.g., the terms $x_i x_j$ and $x_j x_i$ appear twice in the product $\mathbf{x} \otimes \mathbf{x}$. These symmetries are known by construction (12) and can be handled properly. Nevertheless, taking care of these symmetries, the quadratic operator is not a unique representation of the original system, with its entries being not fully detectable, when using only information from the 2nd kernel. Algebraically, this can be explained by the rank deficiency of the least square matrix $\mathbf{M} \in \mathbb{R}^{k \times r^3}$. Further, real symmetry can be enforced in (30) by including the conjugate counterparts. The above problem motivates the usage of higher harmonics (kernels) where the remaining parameters of the above under-determined problem can be estimated. In particular, evaluating the quadratic operator $\hat{\mathbf{Q}}$ can be parameterized further with the non-empty null space that we have computed from the above least-squares problem.

The quadratic operator has r^3 unknowns (less due to symmetries). If the rank of the matrix \mathbf{M} is $\text{rank}(\mathbf{M}) = p < r^3$, the parametric solution of $\hat{\mathbf{Q}}$ that we obtain from H_2 measurements with the dimension of the kernel $m = r^3 - p$ can be written as:

$$\hat{\mathbf{Q}} = \underbrace{\hat{\mathbf{Q}}_s + \hat{\mathbf{Q}}_k}_{\text{rank solution}} + \underbrace{\sum_{i=1}^m \lambda_i \hat{\mathbf{Q}}_i}_{\text{parameterization}} \quad (31)$$

The above splitting (31) can be considered the same when the operators $\hat{\mathbf{Q}}_s, \hat{\mathbf{Q}}_i, i = 1, \dots, m$ are represented as vectors after vectorization due to the linear property of $\text{vec}(\cdot)^2$.

2.5.3. The quadratic operator from the 3rd kernel

From the parameters λ_i in (31), we search those that explain the interpolation of the 3rd kernel as well. Therefore, we can write:

$$\hat{H}_3(s_1, s_2, s_3) = \hat{\mathbf{O}}_3(s_1, s_2, s_3) \hat{\mathbf{Q}} \hat{\mathbf{R}}_3(s_1, s_2, s_3, \hat{\mathbf{Q}}), \quad (32)$$

and substituting (31) in (32), due to the linear property of the operator $\hat{\mathbf{R}}_3$ as explained in section 2.4.1, we can derive

$$\begin{aligned} \hat{H}_3(s_1, s_2, s_3) &= \hat{\mathbf{O}}_3(s_1, s_2, s_3) \left(\hat{\mathbf{Q}}_s + \sum_{i=1}^m \lambda_i \hat{\mathbf{Q}}_i \right) \hat{\mathbf{R}}_3 \left(s_1, s_2, s_3, \hat{\mathbf{Q}}_s + \sum_{i=1}^m \lambda_i \hat{\mathbf{Q}}_i \right) = \\ &= \hat{\mathbf{O}}_3(s_1, s_2, s_3) \hat{\mathbf{Q}}_s \hat{\mathbf{R}}_3 \left(s_1, s_2, s_3, \hat{\mathbf{Q}}_s \right) + \hat{\mathbf{O}}_3(s_1, s_2, s_3) \hat{\mathbf{Q}}_s \hat{\mathbf{R}}_3 \left(s_1, s_2, s_3, \sum_{i=1}^m \lambda_i \hat{\mathbf{Q}}_i \right) + \\ &\hat{\mathbf{O}}_3(s_1, s_2, s_3) \left(\sum_{i=1}^m \lambda_i \hat{\mathbf{Q}}_i \right) \hat{\mathbf{R}}_3 \left(s_1, s_2, s_3, \hat{\mathbf{Q}}_s \right) + \hat{\mathbf{O}}_3(s_1, s_2, s_3) \left(\sum_{i=1}^m \lambda_i \hat{\mathbf{Q}}_i \right) \hat{\mathbf{R}}_3 \left(s_1, s_2, s_3, \sum_{i=1}^m \lambda_i \hat{\mathbf{Q}}_i \right) \\ &= \hat{H}_3^{ss}(s_1, s_2, s_3) + \sum_{i=1}^m \lambda_i \left(\hat{H}_3^{s_i s}(s_1, s_2, s_3) + \hat{H}_3^{s_i i}(s_1, s_2, s_3) \right) + \sum_{i=1}^m \sum_{j=1}^m \lambda_i \lambda_j \hat{H}_3^{ij}(s_1, s_2, s_3), \end{aligned} \quad (33)$$

²The vectorization is row-wise, $\text{vec}(\mathbf{Q}) = [\mathbf{Q}(1, 1 : r^2) \quad \dots \quad \mathbf{Q}(r, 1 : r^2)]^T \in \mathbb{R}^{r^3 \times 1}$.

where, the superscript notation is similar to (27). The above problem can be written as a classical quadratic optimization problem. We introduce the following notation: $\mathcal{A} = \hat{H}_3^{(ij)}(s_1, s_2, s_3)$, $\mathcal{B} = \hat{H}_3^{(is)}(s_1, s_2, s_3) + \hat{H}_3^{(si)}(s_1, s_2, s_3)$, $\mathcal{C} = \hat{H}_3^{(ss)}(s_1, s_2, s_3) - \hat{H}_3(s_1, s_2, s_3)$. We reformulate the problem by denoting $\boldsymbol{\lambda} = [\lambda_1 \ \lambda_2 \ \cdots \ \lambda_m]^T$. The dimensions for a single measurement triplet (s_1, s_2, s_3) remain: $\mathcal{A} \in \mathbb{R}^{n \times n}$, $\mathcal{B} \in \mathbb{R}^{1 \times n}$, $\mathcal{C} \in \mathbb{R}$.

$$\boldsymbol{\lambda}^T \mathcal{A} \boldsymbol{\lambda} + \mathcal{B} \boldsymbol{\lambda} + \mathcal{C} = 0. \quad (34)$$

We can rewrite the above vector equation in a more convenient format after vectorizing \mathcal{A} as:

$$\text{vec}(\mathcal{A})(\boldsymbol{\lambda} \otimes \boldsymbol{\lambda}) + \mathcal{B} \boldsymbol{\lambda} + \mathcal{C} = 0. \quad (35)$$

To enforce interpolation from the 3rd kernel, we equate

$$\underbrace{H_3(s_1^{(k)}, s_2^{(k)}, s_3^{(k)})}_{\text{k: measurements}} = \hat{H}_3(s_1^{(k)}, s_2^{(k)}, s_3^{(k)}). \quad (36)$$

Further, by adding k measurements, we result to:

$$\underbrace{\begin{bmatrix} \text{vec}(\mathcal{A}_1) \\ \text{vec}(\mathcal{A}_2) \\ \vdots \\ \text{vec}(\mathcal{A}_k) \end{bmatrix}}_{\mathbf{W}: (k \times m^2)} (\boldsymbol{\lambda} \otimes \boldsymbol{\lambda}) + \underbrace{\begin{bmatrix} \mathcal{B}_1 \\ \mathcal{B}_2 \\ \vdots \\ \mathcal{B}_k \end{bmatrix}}_{\mathbf{Z}: (k \times m)} \boldsymbol{\lambda} + \underbrace{\begin{bmatrix} \mathcal{C}_1 \\ \mathcal{C}_2 \\ \vdots \\ \mathcal{C}_k \end{bmatrix}}_{\mathbf{S}: (k \times 1)} = \mathbf{0}. \quad (37)$$

The above mapping can be written by denoting $\mathbf{F}(\cdot) : \mathbb{R}^m \rightarrow \mathbb{R}^k$ as $\mathbf{F}(\boldsymbol{\lambda}) = \mathbf{0}$ where:

$$\mathbf{F}(\boldsymbol{\lambda}) = \mathbf{W}(\boldsymbol{\lambda} \otimes \boldsymbol{\lambda}) + \mathbf{Z} \boldsymbol{\lambda} + \mathbf{S}, \quad \boldsymbol{\lambda} \in \mathbb{R}^m. \quad (38)$$

The derivative (Jacobian) w.r.t the real vector $\boldsymbol{\lambda}$ is:

$$\mathbf{J}(\boldsymbol{\lambda}) = \mathbf{F}'(\boldsymbol{\lambda}) = \mathbf{W}(\boldsymbol{\lambda} \otimes \mathbf{I} + \mathbf{I} \otimes \boldsymbol{\lambda}) + \mathbf{Z}. \quad (39)$$

We seek the solution of (37), thus, by introducing the Newton iterative procedure (fixed point iterations), we can conclude in the following scheme where an initial seed $\boldsymbol{\lambda}_0$ can result to $\mathcal{F}(\boldsymbol{\lambda}_{n+1}) \rightarrow 0$ as $n \rightarrow \infty$. The iterations are described next:

$$\boldsymbol{\lambda}_{n+1} = \boldsymbol{\lambda}_n - \mathbf{J}^{-1}(\boldsymbol{\lambda}_n) \mathbf{F}(\boldsymbol{\lambda}_n). \quad (40)$$

Finally, upon Newton's method convergence, we obtain the vector $\boldsymbol{\lambda}^*$, ($\mathbf{F}(\boldsymbol{\lambda}^*) \approx \mathbf{0}$) from algorithm 1, which will lead to a better estimation of \mathbf{Q} that explains, in addition, the measurements from the 3rd kernel. We notice in many situations that the error between the reduced and original systems improves significantly when the residual γ of the Newton's method remains small. Moreover, in many cases, identifying the original operator \mathbf{Q} is possible as we will illustrate in the following example with the Lorenz attractor model.

2.5.4. The algorithm for quadratic modeling from i/o time-domain data

Here, we present a concise algorithm that summarizes the procedure for constructing quadratic state space models from harmonic data (samples of the symmetric kernels H_1 , H_2 , H_3). Measuring (symmetric) Volterra kernels is by no means, a new topic. However, although previously addressed in [16, 37, 54], it still remains a non-trivial task. The main difficulty has to do with the fact that it is hard to separate commensurate frequencies. In other words, each one of the propagating harmonics consists

Algorithm 1 Solution λ of the quadratic vector equation $\mathbf{F}(\lambda) = \mathbf{0}$.

Define: $\mathbf{W} \in \mathbb{R}^{k \times m^2}$, $\mathbf{Z} \in \mathbb{R}^{k \times m}$, $\mathbf{S} \in \mathbb{R}^{k \times 1}$ and the hyperparameters η , γ_0 .
 Choose an initial random seed: $\lambda \in \mathbb{R}^m$.
while $\gamma > \gamma_0$ **do**
 Compute $\mathbf{F}(\lambda)$ from (38) and $\mathbf{J}(\lambda)$ from (39).
 Update $\lambda \leftarrow (\lambda - \mathbf{J}^\# \mathbf{F}(\lambda))$, # is: " - 1" or the Moore-Penrose pseudo-inverse (threshold η).
 Compute the residue $\|\mathbf{F}(\lambda)\| = \gamma$.
end while
return λ

of a series of kernels and, therefore, evaluating the symmetric GFRFs requires kernel separation with an amplitude shifting [37, 54]. Towards this aim, X-parameters in [52], and the references within, represent a direct generalization of the classical S-parameters (for linear dynamics) to the nonlinear case. With this agile machinery, estimations of the higher Volterra kernel can be made in a true engineering setup as in [54] and quadratic state-space surrogate model can be inferred from the proposed method. The next algorithm can use such information (from the X-parameters) to construct quadratic interpretable models.

Algorithm 2 Quadratic modeling from time-domain data

Input: # Measurements of the symmetric GFRFs $H_1(s_1)$, $H_2(s_1, s_2)$, $H_3(s_1, s_2, s_3)$.
 Define a truncation order r with SVD from the Loewner matrix \mathbb{L} (minimal linear).
 Realize the minimal linear subsystem $(\hat{\mathbf{A}}, \hat{\mathbf{B}}, \hat{\mathbf{C}})$ of order r .
 Estimate the $\hat{\mathbf{Q}}_s \in \mathbb{R}^{r \times r^2}$ from (30) by minimizing the 2-norm error (least-squares).
 Update the $\hat{\mathbf{Q}} \in \mathbb{R}^{r \times r^2}$ from (31) after solving (40) with algorithm 3.
return the quadratic model with operators $(\hat{\mathbf{A}}, \hat{\mathbf{Q}}, \hat{\mathbf{B}}, \hat{\mathbf{C}})$.

2.6. Quadratic state-space systems with multiple equilibrium points

Quadratic systems can bifurcate to different equilibrium points that operate locally. Thus, when measuring, multi-operational points can be revealed. To illustrate this phenomenon mathematically, we write the quadratic system (11) after shifting it with the non-zero equilibrium state \mathbf{x}_e . We denote the new state variable $\tilde{\mathbf{x}}(t) = \mathbf{x}(t) - \mathbf{x}_e$, and it remains

$$\begin{aligned}
 \dot{\mathbf{x}}(t) &= \mathbf{A}\mathbf{x}(t) + \mathbf{Q}(\mathbf{x}(t) \otimes \mathbf{x}(t)) + \mathbf{B}u(t) \Rightarrow \\
 \dot{\tilde{\mathbf{x}}}(t) &= \mathbf{A}(\tilde{\mathbf{x}}(t) + \mathbf{x}_e) + \mathbf{Q}((\tilde{\mathbf{x}}(t) + \mathbf{x}_e) \otimes (\tilde{\mathbf{x}}(t) + \mathbf{x}_e)) + \mathbf{B}u(t) \Rightarrow \\
 \dot{\tilde{\mathbf{x}}}(t) &= \mathbf{A}\tilde{\mathbf{x}}(t) + 2\mathbf{Q}(\mathbf{x}_e \otimes \tilde{\mathbf{x}}(t)) + \mathbf{Q}(\tilde{\mathbf{x}}(t) \otimes \tilde{\mathbf{x}}(t)) + \mathbf{A}\mathbf{x}_e + \mathbf{Q}(\mathbf{x}_e \otimes \mathbf{x}_e) + \mathbf{B}u(t) \Rightarrow \\
 \dot{\tilde{\mathbf{x}}}(t) &= \underbrace{(\mathbf{A} + 2\mathbf{Q}(\mathbf{x}_e \otimes \mathbf{I}))}_{\hat{\mathbf{A}}} \tilde{\mathbf{x}}(t) + \mathbf{Q}(\tilde{\mathbf{x}}(t) \otimes \tilde{\mathbf{x}}(t)) + \underbrace{\mathbf{A}\mathbf{x}_e + \mathbf{Q}(\mathbf{x}_e \otimes \mathbf{x}_e)}_{\hat{\mathbf{L}}} + \mathbf{B}u(t).
 \end{aligned} \tag{41}$$

Note that $\mathbf{L} := \mathbf{A}\mathbf{x}_e + \mathbf{Q}(\mathbf{x}_e \otimes \mathbf{x}_e) = \mathbf{0}$, and should remain zero as in the absence of the controller $u(t)$, and with zero initial conditions e.g., $\mathbf{x}_0 = \mathbf{0}$, there is no energy in the system to dissipate. We do not address situations with a limit circle e.g., systems with purely imaginary eigenvalues, for which such systems describe self-sustained dynamics. As a result, the quadratic system that we measure after reaching the equilibrium state \mathbf{x}_e is the following:

$$\begin{cases} \dot{\tilde{\mathbf{x}}}(t) = \hat{\mathbf{A}}\tilde{\mathbf{x}}(t) + \mathbf{Q}(\tilde{\mathbf{x}}(t) \otimes \tilde{\mathbf{x}}(t)) + \mathbf{B}u(t), \\ y(t) = \mathbf{C}\tilde{\mathbf{x}}(t) + \mathbf{C}\mathbf{x}_e. \end{cases} \tag{42}$$

Remark 2.1 (Invariant operators under bifurcations). *The system in (42) suggests that around the new equilibrium state point \mathbf{x}_e , the operators $(\mathbf{Q}, \mathbf{B}, \mathbf{C})$ stay invariant and only the linear operator changes to $\tilde{\mathbf{A}} = \mathbf{A} + 2\mathbf{Q}(\mathbf{x}_e \otimes \mathbf{I})$, along with the DC³ term $\mathbf{C}\mathbf{x}_e$. Therefore, for the multiple equilibrium case, these local systems contain the same invariant information w.r.t. the operators $(\mathbf{Q}, \mathbf{B}, \mathbf{C})$ except the linear operator plus a translation. In other words, the generalized Markov parameters of the system that contain only the operators $(\mathbf{Q}, \mathbf{B}, \mathbf{C})$ are the same around any arbitrary equilibrium \mathbf{x}_e to which the original system bifurcates and any arbitrary coordinate system.*

Two equilibrium points case: Let assume that the original quadratic model has bifurcated to the two different equilibrium points $\hat{\mathbf{x}}_e^{(1)}$, $\check{\mathbf{x}}_e^{(2)}$ and in the different coordinates denoted $(\hat{\mathbf{x}}, \check{\mathbf{x}})$, that explain the dynamical behavior locally. We can write

$$\begin{cases} \dot{\hat{\mathbf{x}}}_1(t) = \hat{\mathbf{A}}_1 \hat{\mathbf{x}}_1(t) + \hat{\mathbf{Q}}_1(\hat{\mathbf{x}}_1(t) \otimes \hat{\mathbf{x}}_1(t)) + \hat{\mathbf{B}}_1 u(t), \\ y_1(t) = \hat{\mathbf{C}}_1 \hat{\mathbf{x}}_1(t), \hat{\mathbf{x}}_1(0) = \mathbf{0}. \end{cases}, \begin{cases} \dot{\check{\mathbf{x}}}_2(t) = \check{\mathbf{A}}_2 \check{\mathbf{x}}_2(t) + \check{\mathbf{Q}}_2(\check{\mathbf{x}}_2(t) \otimes \check{\mathbf{x}}_2(t)) + \check{\mathbf{B}}_2 u(t), \\ y_2(t) = \check{\mathbf{C}}_2 \check{\mathbf{x}}_2(t), \check{\mathbf{x}}_2(0) = \mathbf{0}. \end{cases} \quad (43)$$

Some properties:

- For the first system in (43) holds

$$\underbrace{\hat{\mathbf{A}}_1}_{\text{local}} = \underbrace{\mathbf{A}_1}_{\text{global}} + 2\hat{\mathbf{Q}}_1(\hat{\mathbf{x}}_e^{(1)} \otimes \mathbf{I}) \quad (44)$$

- For the second system in (43) holds

$$\underbrace{\check{\mathbf{A}}_2}_{\text{local}} = \underbrace{\mathbf{A}_2}_{\text{global}} + 2\check{\mathbf{Q}}_2(\check{\mathbf{x}}_e^{(2)} \otimes \mathbf{I}) \quad (45)$$

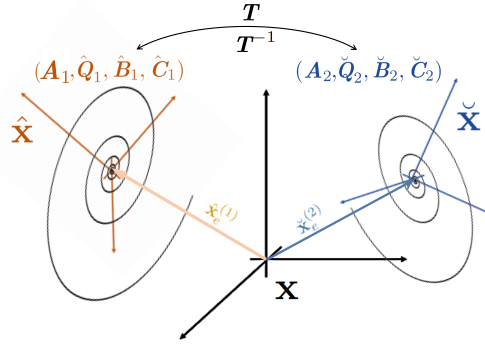


Figure 1: lemma 2.1 through a schematic.

Remark 2.2. *The Markov parameters that involve the quadratic along with the input-output operators are the same. $\hat{\mathbf{C}}_1 \hat{\mathbf{B}}_1 = \check{\mathbf{C}}_2 \check{\mathbf{B}}_2$, and $\hat{\mathbf{C}}_1 \hat{\mathbf{Q}}_1(\hat{\mathbf{B}}_1 \otimes \hat{\mathbf{B}}_1) = \check{\mathbf{C}}_2 \check{\mathbf{Q}}_2(\check{\mathbf{B}}_2 \otimes \check{\mathbf{B}}_2)$.*

According to remark 2.2, invariant information from the original system is encoded in both systems (43). Therefore, there exists a similarity transformation \mathbf{T} which aligns the two systems w.r.t the original operators.

³DC: direct current in electrical engineering, which describes the non-periodic term (zero frequency) in the power spectrum.

Lemma 2.1. *There exists a transformation matrix \mathbf{T} such that the two triplets of operators given by $(\hat{\mathbf{Q}}_1, \hat{\mathbf{B}}_1, \hat{\mathbf{C}}_1)$ and by $(\check{\mathbf{Q}}_2, \check{\mathbf{B}}_2, \check{\mathbf{C}}_2)$ (resulting after a global model bifurcating to different equilibrium points) can be aligned simultaneously with the original operators but to different coordinates, geometrically in [fig. 1](#), and algebraically as*

$$\begin{aligned}\hat{\mathbf{Q}}_1 &= \mathbf{T}\check{\mathbf{Q}}_2(\mathbf{T}^{-1} \otimes \mathbf{T}^{-1}), \\ \hat{\mathbf{B}}_1 &= \mathbf{T}^{-1}\check{\mathbf{B}}_2 \Leftrightarrow \mathbf{T}\hat{\mathbf{B}}_1 = \check{\mathbf{B}}_2 \\ \hat{\mathbf{C}}_1 &= \mathbf{T}\check{\mathbf{C}}_2, \\ \mathbf{A}_1 &= \mathbf{T}\mathbf{A}_2\mathbf{T}^{-1}.\end{aligned}\tag{46}$$

One way to compute the transformation matrix \mathbf{T} is by solving the first three equations in system [\(46\)](#). The above problem involves a quadratic matrix equation that can be iteratively solved by means of Newton iterations. Moreover, the linear constraints help the regularization of the Newton iterations not to converge at the zero solution. To seek such a formal solution we analytically derive the iterative Newton scheme over the Fréchet derivative in what follows ([section 2.7](#)).

2.7. Solution of the constrained quadratic matrix equation

The analysis starts with the quadratic matrix equation, thus we define the following operator: $\mathcal{F} : \mathbb{R}^{n \times n} \rightarrow \mathbb{R}^{n \times n}$ with $\mathcal{F}(\mathbf{X}) := \mathbf{X}\mathbf{U} - \mathbf{Q}(\mathbf{X} \otimes \mathbf{X})$. For known \mathbf{U} , $\mathbf{Q} \in \mathbb{R}^{n \times n^2}$, we seek $\mathbf{0} \neq \mathbf{X} \in \mathbb{R}^{n \times n}$ such that $\mathcal{F}(\mathbf{X}) = \mathbf{0}$. Moreover, \mathbf{X} should be invertible ($\exists \mathbf{X}^{-1}$). The idea is to differentiate w.r.t. the Fréchet derivative and solve a linear matrix equation for every Newton step similar to the Newton-Kleinmann algorithm for the solution of the Riccati matrix equation [\[40\]](#). Therefore, we introduce a small perturbation to the matrix \mathbf{X} with $\mathbf{N} \in \mathbb{R}^{n \times n}$ and with h a small real number. We define

$$(\mathcal{F}'(\mathbf{X}))(\mathbf{N}) = \lim_{h \rightarrow 0} \frac{1}{h} (\mathcal{F}(\mathbf{X} + h\mathbf{N}) - \mathcal{F}(\mathbf{X})) = \mathbf{N}\mathbf{U} - \mathbf{Q}(\mathbf{X} \otimes \mathbf{N} + \mathbf{N} \otimes \mathbf{X}).\tag{47}$$

Since \mathbf{Q} is symmetric, we can write equivalently

$$(\mathcal{F}'(\mathbf{X}))(\mathbf{N}) = \mathbf{N}\mathbf{U} - 2\mathbf{Q}(\mathbf{X} \otimes \mathbf{N}).\tag{48}$$

The Newton iteration is given by

$$(\mathcal{F}'(\mathbf{X}_{j-1}))(\mathbf{N}_{j-1}) = -\mathcal{F}(\mathbf{X}_{j-1}), \quad \mathbf{X}_j = \mathbf{X}_{j-1} + \mathbf{N}_{j-1}.\tag{49}$$

We compute

$$\begin{aligned}\mathbf{N}_{j-1}\mathbf{U} - 2\mathbf{Q}(\mathbf{X}_{j-1} \otimes \mathbf{N}_{j-1}) &= -\mathbf{X}_{j-1}\mathbf{U} + \mathbf{Q}(\mathbf{X}_{j-1} \otimes \mathbf{X}_{j-1}) \Rightarrow \\ (\mathbf{X}_j - \mathbf{X}_{j-1})\mathbf{U} - 2\mathbf{Q}(\mathbf{X}_{j-1} \otimes (\mathbf{X}_j - \mathbf{X}_{j-1})) &= -\mathbf{X}_{j-1}\mathbf{U} + \mathbf{Q}(\mathbf{X}_{j-1} \otimes \mathbf{X}_{j-1}) \Rightarrow \\ \mathbf{X}_j\mathbf{U} - 2\mathbf{Q}(\mathbf{X}_{j-1} \otimes \mathbf{X}_j) + 2\mathbf{Q}(\mathbf{X}_{j-1} \otimes \mathbf{X}_{j-1}) &= \mathbf{Q}(\mathbf{X}_{j-1} \otimes \mathbf{X}_{j-1})\end{aligned}\tag{50}$$

which results to the following linear matrix equation [\(51\)](#) w.r.t the forward step solution \mathbf{X}_j :

$$\mathbf{X}_j\mathbf{U} - 2\mathbf{Q}(\mathbf{X}_{j-1} \otimes \mathbf{X}_j) + \mathbf{Q}(\mathbf{X}_{j-1} \otimes \mathbf{X}_{j-1}) = 0.\tag{51}$$

Remark 2.3. *In [\(51\)](#), it is to be observed that at step j , the matrix equation is actually linear in \mathbf{X}_j , provided that \mathbf{X}_{j-1} is explicitly known, which is to be assumed (from the Newton iteration).*

Remark 2.4. *The equation [\(51\)](#) is linear in the variable $\mathbf{X}_j \in \mathbb{R}^{n \times n}$; since $\mathbf{U}, \mathbf{Q} \in \mathbb{R}^{n \times n^2}$, there are n^3 linear scalar equations to solve, and only n^2 unknowns. Hence, we are facing an over-determined linear system of equations with a possibly non-empty null space.*

In what follows we show how to isolate the \mathbf{X}_j term from the rest, and how to re-write this equation in a more conventional way. More specifically, based on the previous remark, we show that equation (51) can equivalently be written as n classical Sylvester equations, each characterized by n^2 scalar equations in n^2 unknowns. From (51), it follows that

$$\begin{aligned} \mathbf{X}_j \mathbf{U} - 2\mathbf{Q}(\mathbf{X}_{j-1} \otimes \mathbf{X}_j) + \mathbf{Q}(\mathbf{X}_{j-1} \otimes \mathbf{X}_{j-1}) &= 0 \Rightarrow \\ \mathbf{X}_j \mathbf{U} - \underbrace{2\mathbf{Q}(\mathbf{X}_{j-1} \otimes \mathbf{I}_n)}_{:=\mathbf{V}_{j-1}} (\mathbf{I}_n \otimes \mathbf{X}_j) &= \underbrace{-\mathbf{Q}(\mathbf{X}_{j-1} \otimes \mathbf{X}_{j-1})}_{:=\mathbf{Z}_{j-1}} \Rightarrow \end{aligned} \quad (52)$$

$$\mathbf{X}_j \underbrace{[\mathbf{U}^{(1)} \ \dots \ \mathbf{U}^{(n)}]}_{\mathbf{U}} - \underbrace{[\mathbf{V}_{j-1}^{(1)} \ \dots \ \mathbf{V}_{j-1}^{(n)}]}_{\mathbf{V}_{j-1}} \begin{bmatrix} \mathbf{X}_j & \mathbf{0} & \dots & \mathbf{0} \\ \mathbf{0} & \mathbf{X}_j & \dots & \mathbf{0} \\ \vdots & \vdots & \ddots & \vdots \\ \mathbf{0} & \mathbf{0} & \dots & \mathbf{X}_j \end{bmatrix} = \underbrace{[\mathbf{Z}_{j-1}^{(1)} \ \mathbf{Z}_{j-1}^{(2)} \ \dots \ \mathbf{Z}_{j-1}^{(n)}]}_{\mathbf{Z}_{j-1}}. \quad (53)$$

Above, we have that $\mathbf{U}^{(k)}$, $\mathbf{V}_{j-1}^{(k)}$, $\mathbf{Z}_{j-1}^{(k)}$ are known $n \times n$ real-valued matrices at step j , for all $1 \leq k \leq n$. These are actually the building blocks of the following matrices:

$$\mathbf{V}_{j-1} := 2\mathbf{Q}(\mathbf{X}_{j-1} \otimes \mathbf{I}_n) \in \mathbb{R}^{n \times n^2}, \quad \mathbf{Z}_{j-1} := -\mathbf{Q}(\mathbf{X}_{j-1} \otimes \mathbf{X}_{j-1}) \in \mathbb{R}^{n \times n^2}. \quad (54)$$

We can hence write this equation, equivalently as follows:

$$[\mathbf{X}_j \mathbf{U}^{(1)} \ \dots \ \mathbf{X}_j \mathbf{U}^{(n)}] - [\mathbf{V}_{j-1}^{(1)} \ \dots \ \mathbf{V}_{j-1}^{(n)} \mathbf{X}_j] = [\mathbf{Z}_{j-1}^{(1)} \ \dots \ \mathbf{Z}_{j-1}^{(n)}]. \quad (55)$$

Then, for all $1 \leq k \leq n$, solving (51) boils down to solving n (linear) Sylvester equations as:

$$\mathbf{X}_j \mathbf{U}^{(k)} - \mathbf{V}_{j-1}^{(k)} \mathbf{X}_j = \mathbf{Z}_{j-1}^{(k)}. \quad (56)$$

The solution $\mathbf{X}_j \in \mathbb{R}^{n \times n}$, after vectorization, becomes $\text{vec}(\mathbf{X}_j) \in \mathbb{R}^{n^2 \times 1}$. Putting together the n Sylvester equations in vectorized form by using the identity $\text{vec}(\mathbf{TOR}) = (\mathbf{R}^T \otimes \mathbf{T})\text{vec}(\mathbf{O})$, will yield the following system of n^3 scalar equations in n^2 unknowns:

$$\underbrace{\begin{bmatrix} (\mathbf{U}^{(1)})^T \otimes \mathbf{I}_n - \mathbf{I}_n \otimes \mathbf{V}_{j-1}^{(1)} \\ (\mathbf{U}^{(2)})^T \otimes \mathbf{I}_n - \mathbf{I}_n \otimes \mathbf{V}_{j-1}^{(2)} \\ \vdots \\ (\mathbf{U}^{(n)})^T \otimes \mathbf{I}_n - \mathbf{I}_n \otimes \mathbf{V}_{j-1}^{(n)} \end{bmatrix}}_{\in \mathbb{R}^{n^3 \times n^2}} \text{vec}(\mathbf{X}_j) = \underbrace{\begin{bmatrix} \text{vec}(\mathbf{Z}_{j-1}^{(1)}) \\ \text{vec}(\mathbf{Z}_{j-1}^{(2)}) \\ \vdots \\ \text{vec}(\mathbf{Z}_{j-1}^{(n)}) \end{bmatrix}}_{\in \mathbb{R}^{n^3 \times 1}} \quad (57)$$

For low values of n , such a procedure is indeed feasible. However, for moderate to large values of n , i.e., $n > 50$ or so, it is quite challenging or even impossible to find the next value \mathbf{X}_j , by means of explicitly forming the $n^3 \times n^2$ matrix in (57). In what follows, we are concerned with low-order systems as we are emphasizing quadratic identification in a reduced-order sense.

Lemma 2.2. *The square matrix \mathbf{T}^{-1} that aligns the operators $(\hat{\mathbf{Q}}_1, \hat{\mathbf{B}}_1, \hat{\mathbf{C}}_1)$ and $(\check{\mathbf{Q}}_2, \check{\mathbf{B}}_2, \check{\mathbf{C}}_2)$ from lemma 2.1, can be computed, upon Newton's method convergence algorithm 3, as the iterative solution of the following constrained linear system of equations (58) with $\mathbf{T}^{-1} := \lim_{j \rightarrow \infty} \mathbf{X}_j$ that gives $\mathcal{F}(\mathbf{T}^{-1}) \approx \mathbf{0}$.*

$$\underbrace{\begin{bmatrix} (\mathbf{U}^{(1)})^T \otimes \mathbf{I}_n - \mathbf{I}_n \otimes \mathbf{V}_{j-1}^{(1)} \\ (\mathbf{U}^{(2)})^T \otimes \mathbf{I}_n - \mathbf{I}_n \otimes \mathbf{V}_{j-1}^{(2)} \\ \vdots \\ (\mathbf{U}^{(n)})^T \otimes \mathbf{I}_n - \mathbf{I}_n \otimes \mathbf{V}_{j-1}^{(n)} \\ \hat{\mathbf{B}}_1^T \otimes \mathbf{I}_n \\ \mathbf{I}_n \otimes \check{\mathbf{C}}_2 \end{bmatrix}}_{\in \mathbb{R}^{(n^3+2n) \times n^2}} \text{vec}(\mathbf{X}_j) = \underbrace{\begin{bmatrix} \text{vec}(\mathbf{Z}_{j-1}^{(1)}) \\ \text{vec}(\mathbf{Z}_{j-1}^{(2)}) \\ \vdots \\ \text{vec}(\mathbf{Z}_{j-1}^{(n)}) \\ \mathbf{B}_2 \\ \hat{\mathbf{C}}_1^T \end{bmatrix}}_{\in \mathbb{R}^{(n^3+2n) \times 1}} \quad (58)$$

Algorithm 3 Solution of the constrained quadratic matrix equation with Newton method

Seek: \mathbf{X} s.t. $\mathcal{F}(\mathbf{X}) := \mathbf{X}\mathbf{U} - \mathbf{Q}(\mathbf{X} \otimes \mathbf{X}) = \mathbf{0}$ and satisfies the constrains (two last rows) in (58).

Choose an initial random seed: $\mathbf{X}_{j=0} \in \mathbb{R}^{n \times n}$.

while $\gamma > \gamma_0$ **do**

 Update: $j \leftarrow j + 1$.

 Compute \mathbf{X}_j by solving the linear system of equations (58).

 Compute the residue $\|\mathcal{F}(\mathbf{X}_j)\| = \gamma$.

end while

return \mathbf{X}

With the solution \mathbf{T}^{-1} from algorithm 3, we can align the "hatted" and "breved" systems to the same coordinates. We can further write after combining equations (44) and (45), the following system with unknowns the equilibrium state points $\hat{\mathbf{x}}_e^{(1)}$, $\check{\mathbf{x}}_e^{(2)}$. Combining equations (44) and (45) after multiplication with the transformation matrix \mathbf{T} from the left and with \mathbf{T}^{-1} from the right, we have

$$\begin{aligned}
 \check{\mathbf{A}}_2 &= \mathbf{A}_2 + 2\check{\mathbf{Q}}_2(\check{\mathbf{x}}_e^{(2)} \otimes \mathbf{I}) \Rightarrow \\
 \mathbf{T}\check{\mathbf{A}}_2\mathbf{T}^{-1} &= \mathbf{T}\mathbf{A}_2\mathbf{T}^{-1} + 2\mathbf{T}\check{\mathbf{Q}}_2(\check{\mathbf{x}}_e^{(2)} \otimes \mathbf{I})\mathbf{T}^{-1} \Rightarrow \\
 \mathbf{T}\check{\mathbf{A}}_2\mathbf{T}^{-1} &= \mathbf{A}_1 + 2\mathbf{T}\check{\mathbf{Q}}_2(\check{\mathbf{x}}_e^{(2)} \otimes \mathbf{T}^{-1}) \Rightarrow \\
 \mathbf{T}\check{\mathbf{A}}_2\mathbf{T}^{-1} &= \mathbf{A}_1 + 2\mathbf{T}\check{\mathbf{Q}}_2(\mathbf{T}^{-1} \otimes \mathbf{T}^{-1})(\mathbf{T}^{-1} \otimes \mathbf{T}^{-1})^{-1}(\check{\mathbf{x}}_e^{(2)} \otimes \mathbf{T}^{-1}) \\
 \mathbf{T}\check{\mathbf{A}}_2\mathbf{T}^{-1} &= \mathbf{A}_1 + 2\hat{\mathbf{Q}}_1(\mathbf{T}^{-1} \otimes \mathbf{T}^{-1})^{-1}(\check{\mathbf{x}}_e^{(2)} \otimes \mathbf{T}^{-1}) \Rightarrow \\
 \mathbf{T}\check{\mathbf{A}}_2\mathbf{T}^{-1} &= \mathbf{A}_1 + 2\hat{\mathbf{Q}}_1(\mathbf{T} \otimes \mathbf{T})(\check{\mathbf{x}}_e^{(2)} \otimes \mathbf{T}^{-1}) \Rightarrow \\
 \mathbf{T}\check{\mathbf{A}}_2\mathbf{T}^{-1} &= \mathbf{A}_1 + 2\hat{\mathbf{Q}}_1(\mathbf{T}\check{\mathbf{x}}_e^{(2)} \otimes \mathbf{I}) \Rightarrow \\
 \mathbf{T}\check{\mathbf{A}}_2\mathbf{T}^{-1} &= \hat{\mathbf{A}}_1 - 2\hat{\mathbf{Q}}_1(\hat{\mathbf{x}}_e^{(1)} \otimes \mathbf{I}) + 2\hat{\mathbf{Q}}_1(\mathbf{T}\check{\mathbf{x}}_e^{(2)} \otimes \mathbf{I}) \Rightarrow \\
 \mathbf{T}\check{\mathbf{A}}_2\mathbf{T}^{-1} &= \hat{\mathbf{A}}_1 - 2\hat{\mathbf{Q}}_1(\hat{\mathbf{x}}_e^{(1)} - \mathbf{T}\check{\mathbf{x}}_e^{(2)} \otimes \mathbf{I}) \Rightarrow \\
 \hat{\mathbf{A}}_1 - \mathbf{T}\check{\mathbf{A}}_2\mathbf{T}^{-1} &= 2\hat{\mathbf{Q}}_1(\hat{\mathbf{x}}_e^{(1)} - \mathbf{T}\check{\mathbf{x}}_e^{(2)} \otimes \mathbf{I}).
 \end{aligned} \tag{59}$$

The above equation is not enough for defining uniquely the unknown equilibrium vectors. Additional information is coming from the direct current (DC) terms that can be measured from the power spectrum α_1 , α_2 . Therefore, we enforce from the table 2

$$\hat{\mathbf{C}}_1\hat{\mathbf{x}}_e^{(1)} = \alpha_1, \quad \check{\mathbf{C}}_2\check{\mathbf{x}}_e^{(2)} = \alpha_2, \tag{60}$$

Solving the coupled system with (59) and (60), we obtain infinite solution of the vectors $\hat{\mathbf{x}}_e^{(1)}$, $\check{\mathbf{x}}_e^{(2)}$ as a non-empty null space of length p exists. Finally, each one of the systems at the equilibrium point satisfies $\mathbf{L} := \mathbf{A}\mathbf{x}_e + \mathbf{Q}(\mathbf{x}_e \otimes \mathbf{x}_e) = \mathbf{0}$. Therefore, working independently, at $\hat{\mathbf{x}}_e^{(1)}$, it holds $\hat{\mathbf{L}}(\hat{\mathbf{x}}_e^{(1)}) = \mathbf{0}$. The solution that we estimate from (59) is not unique due to the rank deficiency. In particular, we have to solve for the two equilibrium points another two quadratic vector equations that enforce $\hat{\mathbf{L}}(\hat{\mathbf{x}}_e^{(1)})$ and $\check{\mathbf{L}}(\check{\mathbf{x}}_e^{(2)})$ equal zero. Therefore, we solve for the parametric solution

$$\begin{bmatrix} \mathbf{x}_e^{(1)} \\ \mathbf{x}_e^{(2)} \end{bmatrix} = \begin{bmatrix} \mathbf{x}_{es}^{(1)} \\ \mathbf{x}_{es}^{(2)} \end{bmatrix} + \sum_{i=1}^p \lambda_i \begin{bmatrix} \mathbf{x}_{ei}^{(1)} \\ \mathbf{x}_{ei}^{(2)} \end{bmatrix}, \tag{61}$$

the following equation for every equilibrium point. Thus,

$$\begin{aligned}
\hat{\mathbf{L}}(\hat{\mathbf{x}}_e^{(1)}) &:= \mathbf{A}_1 \hat{\mathbf{x}}_e^{(1)} + \hat{\mathbf{Q}}_1(\hat{\mathbf{x}}_e^{(1)} \otimes \hat{\mathbf{x}}_e^{(1)}) = \hat{\mathbf{A}}_1 \hat{\mathbf{x}}_e^{(1)} - \hat{\mathbf{Q}}_1(\hat{\mathbf{x}}_e^{(1)} \otimes \hat{\mathbf{x}}_e^{(1)}) = \\
&= \hat{\mathbf{A}}_1 \left(\hat{\mathbf{x}}_{es}^{(1)} + \sum_{i=1}^p \lambda_i \mathbf{x}_{ei}^{(1)} \right) - \hat{\mathbf{Q}}_1 \left(\hat{\mathbf{x}}_{es}^{(1)} + \sum_{i=1}^p \lambda_i \mathbf{x}_{ei}^{(1)} \right) \otimes \left(\hat{\mathbf{x}}_{es}^{(1)} + \sum_{i=1}^p \lambda_i \mathbf{x}_{ei}^{(1)} \right) = \\
&= \underbrace{\hat{\mathbf{A}}_1 \hat{\mathbf{x}}_{es}^{(1)} - \hat{\mathbf{Q}}_1(\hat{\mathbf{x}}_{es}^{(1)} \otimes \hat{\mathbf{x}}_{es}^{(1)})}_{\mathbf{Z}} + \sum_{i=1}^p \lambda_i \underbrace{\left(\hat{\mathbf{A}}_1 \mathbf{x}_{ei}^{(1)} - 2\hat{\mathbf{Q}}_1 \mathbf{x}_{es}^{(1)} \otimes \mathbf{x}_{ei}^{(1)} \right)}_{\mathbf{Y}} - \\
&\quad - \sum_{i=1}^p \sum_{j=1}^p \lambda_i \lambda_j \underbrace{\hat{\mathbf{Q}}_1(\mathbf{x}_{ei}^{(1)} \otimes \mathbf{x}_{ej}^{(1)})}_{\mathbf{W}} = \mathbf{0}.
\end{aligned} \tag{62}$$

Therefore, after enforcing the \mathbf{L} vector to be zero at each equilibrium point and for both systems, we end up solving a system of coupled quadratic vector equations.

$$\begin{bmatrix} \mathbf{W}_1 \\ \mathbf{W}_2 \end{bmatrix} (\boldsymbol{\lambda} \otimes \boldsymbol{\lambda}) + \begin{bmatrix} \mathbf{Y}_1 \\ \mathbf{Y}_2 \end{bmatrix} \boldsymbol{\lambda} + \begin{bmatrix} \mathbf{Z}_1 \\ \mathbf{Z}_2 \end{bmatrix} = \mathbf{0}. \tag{63}$$

Solving for $\boldsymbol{\lambda}$ with the same developed [algorithm 1](#), we can detect uniquely the equilibrium state vectors $\hat{\mathbf{x}}_e^{(1)}$, $\check{\mathbf{x}}_e^{(2)}$. Finally, we can identify the initial system that contains the original operators e.g., \mathbf{A}_1 . In particular, the identified system with operators $(\hat{\mathbf{A}}_1, \hat{\mathbf{Q}}_1, \hat{\mathbf{B}}_1, \hat{\mathbf{C}}_1)$ is an equivalent modulo with the original $(\mathbf{A}, \mathbf{Q}, \mathbf{B}, \mathbf{C})$ and a similarity transformation $\mathbf{T} \in \mathbb{R}^{n \times n}$ exists that aligns the two systems as in the [appendix A](#).

3. Numerical results

We test the new method for different cases of identifying the Lorenz attractor where the Burgers' equation model illustrates the reduction performance.

3.1. Chaotic Lorenz system

We consider the canonical model for chaotic dynamics, the Lorenz system [\[43\]](#) and we add a control-input $u(t)$ in the 1st and 3rd states. The quadratic control system is described by the following state-space form:

$$\begin{cases} \dot{x}(t) = -\sigma x(t) + \sigma y(t) + u(t), \\ \dot{y}(t) = \rho x(t) - y(t) - x(t)z(t), \\ \dot{z}(t) = -\beta z(t) + x(t)y(t) + u(t), \end{cases} \tag{64}$$

where zero initial condition are assumed e.g., $(x(0), y(0), z(0)) = (0, 0, 0)$, and the operators are:

$$\mathbf{A} = \begin{bmatrix} -\sigma & \sigma & 0 \\ \rho & -1 & 0 \\ 0 & 0 & -\beta \end{bmatrix}, \quad \mathbf{B} = \mathbf{C}^T = \begin{bmatrix} 1 \\ 0 \\ 1 \end{bmatrix}, \quad \mathbf{Q} = \begin{bmatrix} 0 & 0 & 0 & 0 & 0 & 0 & 0 & 0 & 0 \\ 0 & 0 & -\frac{1}{2} & 0 & 0 & 0 & -\frac{1}{2} & 0 & 0 \\ 0 & \frac{1}{2} & 0 & \frac{1}{2} & 0 & 0 & 0 & 0 & 0 \end{bmatrix}. \tag{65}$$

With input $u(t)$, we choose to observe the linear combination of the 1st and 3rd states, thus, the output is $x(t) + z(t)$. The above quadratic system [\(65\)](#) gives rise to chaotic dynamics for different choices of the parameters (σ, ρ, β) . The aim of this study is to identify the Lorenz system from i/o time domain data under harmonic excitation. We choose $\sigma = 10$, $\beta = 8/3$, and for the parameter ρ , we investigate two cases 1,2 and comment on case 3.

1. $\rho = 0.5$, where the linear subsystem is stable and the Lorenz attractor has the unique zero equilibrium.
2. $\rho = 20$, where the linear subsystem is unstable and the Lorenz system has two different steady-states with two non-zero stable equilibrium points.

3. $\rho = 28$, where the linear subsystem is unstable but the Lorenz system is chaotic (steady-state unreachable) with two non-trivial attractors.

Case 1 - $\rho = 0.5$. Exciting the Lorenz system (65) with multi-harmonic inputs e.g., $u(t) = a_1 e^{s_1 t} + a_2 e^{s_2 t} + a_3 e^{s_3 t}$, where $j = \sqrt{-1}$ the imaginary unit, and $s_1 = j\omega_1$, $s_2 = j\omega_2$, $s_3 = j\omega_3$, after reaching the steady-state profile, measurements of the GFRFs can be achieved e.g., with X-parameters. The data assimilation process is repetitive and for the real input case e.g., $u(t) = \sum_{i=1}^n \cos(\omega_i t)$, kernel separation should be addressed in a similar way as in [15, 16, 37]. Therefore, samples of the first three GFRFs over the following frequency grids can be obtained from a physical measurement setup after processing the time-domain evolution of the potentially unknown system.

- We take 50 logarithmic distributed measurements ω_i , $i = 1, \dots, 50$, from $[10^{-2}, 10^2]$. Therefore, 50 pairs of measurements $\{j\omega_i, H_1(j\omega_i)\}$, $i = 1, \dots, 50$ are collected. Using the Loewner framework section 2.2, the order $r = 3$ of the linear minimal subsystem can be identified from the singular value decay fig. 2(left), and a linear realization can be constructed:

$$\hat{\mathbf{A}} = \begin{bmatrix} 16.96 & 4.171 & -4.638 \\ 11.32 & 4.408 & -4.287 \\ 135.2 & 29.95 & -35.03 \end{bmatrix}, \quad \hat{\mathbf{B}} = \begin{bmatrix} -3.047 \\ -1.824 \\ -24.97 \end{bmatrix}, \quad \hat{\mathbf{C}}^T = \begin{bmatrix} 2.542 \\ 0.08718 \\ -0.3968 \end{bmatrix}. \quad (66)$$

The coordinate system is different from the original, but the system's invariant quantities are the same e.g., the 1st transfer function H_1 , or Markov parameters e.g., $\mathbf{CAB} = \hat{\mathbf{C}}\hat{\mathbf{A}}\hat{\mathbf{B}} = -12.6667$. The eigenvalues are: $\mathbf{eig}(\mathbf{A}) = \mathbf{eig}(\hat{\mathbf{A}}) = (-10.52 \quad -0.4751 \quad -2.667)$.

- We take 10 logarithmic distributed measurements from a squared grid $[10^{-2}, 10^2]^2$ in each dimension⁴, and 100 pairs of measurements $\{(j\omega_1^k, j\omega_2^k), H_2(j\omega_1^k, j\omega_2^k)\}$ are collected. Solving the linear system (30) by minimizing the 2-norm (least-squares), we estimate $\hat{\mathbf{Q}}_s$ as

$$\hat{\mathbf{Q}}_s = \begin{bmatrix} -1.243 & 0.1493 & 0.2813 & 0.1493 & -0.01241 & 0.01805 & 0.2813 & 0.01805 & -0.05817 \\ 0.1416 & 0.8189 & 0.03877 & 0.8189 & -0.2759 & 0.03372 & 0.03877 & 0.03372 & -0.007071 \\ 0.4246 & 0.03703 & 0.8877 & 0.03703 & 0.1219 & 0.2355 & 0.8877 & 0.2355 & -0.2717 \end{bmatrix}. \quad (67)$$

- The rank of the least squares matrix in (30) is deficient $\mathbf{rank}(\mathbf{M}) = 21 < 27 = 3^3$. Therefore, a parameterization as in (31) is introduced. In this particular case, the dimension of the vector $\boldsymbol{\lambda}$ is six. As the proposed method is arbitrary in the amount of measurements, we take 5 logarithmic distributed measurements from the cubic grid $[10^{-2}, 10^2]^3$ in each dimension, therefore, 125 pairs of measurements $\{(j\omega_1^k, j\omega_2^k, j\omega_3^k), H_3(j\omega_1^k, j\omega_2^k, j\omega_3^k)\}$ are collected. Solving the quadratic equation with algorithm 1, and starting with different seeds of λ_0 , as it is depicted on the right of fig. 2, the parameter vector $\boldsymbol{\lambda} \in \mathbb{R}^6$ is obtained uniquely. Thus, the updated estimation of the quadratic operator $\hat{\mathbf{Q}} = \hat{\mathbf{Q}}_s + \sum_{i=1}^r \lambda \hat{\mathbf{Q}}_i$, with $\hat{\mathbf{Q}}_i$ the null space vectors is the following:

$$\hat{\mathbf{Q}} = \begin{bmatrix} -1.513 & -0.1403 & 0.2603 & -0.1403 & -0.006141 & 0.0241 & 0.2603 & 0.0241 & -0.04477 \\ 22.15 & 0.5147 & -3.506 & 0.5147 & 0.01186 & -0.08085 & -3.506 & -0.08085 & 0.5511 \\ -5.541 & -0.7411 & 0.9982 & -0.7411 & -0.03402 & 0.1284 & 0.9982 & 0.1284 & -0.1794 \end{bmatrix}. \quad (68)$$

Finally, making use of a coordinate transformation, we prove that the resulting system is exactly the original after applying the following transformation Ψ in appendix A.

$$\begin{aligned} \mathbf{A} &= \Psi^{-1} \hat{\mathbf{A}} \Psi = \begin{bmatrix} -10.0 & 10.0 & 4.334e-13 \\ 0.5 & -1.0 & 5.219e-13 \\ -5.254e-11 & 5.448e-11 & -2.667 \end{bmatrix}, \\ \mathbf{B} &= \Psi^{-1} \hat{\mathbf{B}} = \begin{bmatrix} 1.0 \\ -2.207e-11 \\ 1.0 \end{bmatrix}, \quad \mathbf{C} = \hat{\mathbf{C}} \Psi = [1.0 \quad -1.806e-11 \quad 1.0], \\ \mathbf{Q} &= \Psi^{-1} \hat{\mathbf{Q}} (\Psi \otimes \Psi) = \begin{bmatrix} 0 & 0 & 0 & 0 & 0 & 0 & 0 & 0 & 0 \\ 0 & 0 & -0.5 & 0 & 0 & 0 & -0.5 & 0 & 0 \\ 0 & 0.5 & 0 & 0.5 & 0 & 0 & 0 & 0 & 0 \end{bmatrix} + \epsilon \cdot \mathbf{1}^{3 \times 9}, \end{aligned} \quad (69)$$

⁴Cartesian product: $[a, b]^2 = [a, b] \times [a, b]$ for $a < b$.

where $\pm\epsilon \in [1e-12, 1e-10]$. The above result certifies that the original system and the identified one are equivalent under a coordinate transformation (equivalent modulo). Important is also the fact that since $\mathbf{Q} \neq \Psi^{-1} \hat{\mathbf{Q}}_s(\Psi \otimes \Psi)$, quadratic identification with information from the first two kernels H_1, H_2 is impossible even if we have taken measurements with two harmonic input tones (off the diagonal). Here, the significant improvement in comparison with other similar efforts [38] is the systematic way for adding more information to the constructed model from the higher kernels. As a result, the forced Lorenz system was successfully identified when measurements of the first three symmetric kernels were considered as it is illustrated in fig. 3(left) in contrast with the unstable result obtained with information available only from the first two kernels. Finally, in fig. 3(right) the identified and the original systems are equivalent state-space models after comparing them at the same coordinate system.

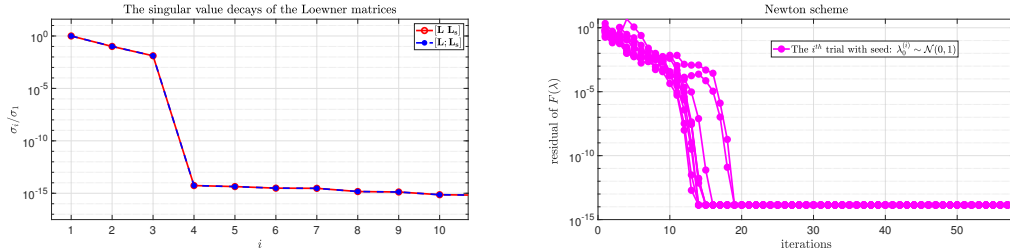


Figure 2: **Left:** The Loewner singular value decay $r = 3$ with $\sigma_4/\sigma_1 \sim 1e - 14$. **Right:** The Newton convergence scheme. A solution vector λ^* has been obtained uniquely and after starting with different random seeds λ_0 .

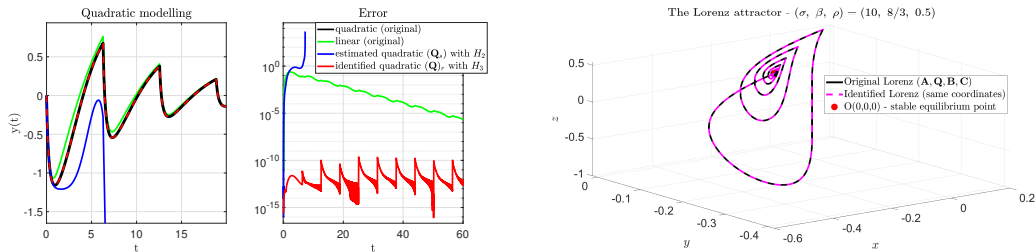


Figure 3: **Left:** The linear model gives a poor approximation. Also, the H_2 does not contribute to a reasonable estimation of the quadratic operator; therefore, numerical instability is observed. After enhancing the information from the 3rd kernel, identification of the Lorenz system has been achieved with numerical error near machine precision. **Right:** The 3D state space is reconstructed from the identified system with the proposed method compared with the original one after aligning both systems to the same coordinates.

Case 2 - $\rho = 20$. For this case where $\rho > 1$, the Lorenz attractor has two non-zero equilibrium points $\mathbf{x}_e^{(1)} = [\sqrt{\beta(\rho-1)} \quad \sqrt{\beta(\rho-1)} \quad \rho-1]^T$ and $\mathbf{x}_e^{(2)} = [-\sqrt{\beta(\rho-1)} \quad -\sqrt{\beta(\rho-1)} \quad \rho-1]^T$. Under harmonic excitation or under non-zero initial conditions, the system's trajectories are moving around these two attractors. The chaotic behavior can be detected from the fact that for small perturbations of the initial conditions or input, the system can switch steady-state making the output evolution totally different.

Data assimilation over multiple steady-states. In table 2, we show for a control system the way that measurements of the higher kernels can be obtained after exciting with harmonic inputs. Here, we illustrate this phenomenon by exciting with harmonic inputs the Lorenz attractor with the parameter

$\rho = 20$. With $\alpha = 1$, $\omega_1 = 1$, we have two different designed complex inputs⁵ that converge to the same input signal for large t .

1. $\rho = 20$ - input 1: $u_1(t) = \underbrace{3e^{-0.1t} \text{sawtooth}(t)}_{\text{perturbation}} + \alpha e^{2j\pi\omega_1 t}$.
2. $\rho = 20$ - input 2: $u_2(t) = \alpha e^{2j\pi\omega_1 t}$.

Clearly, as it is depicted in [fig. 4\(left\)](#), for the different designed inputs $u_1(t)$, $u_2(t)$, we obtain two different steady-state solutions with different power spectrums [fig. 4\(right\)](#). Measurements can be obtained for both systems and the DC terms may help distinguish them. The symmetric transfer

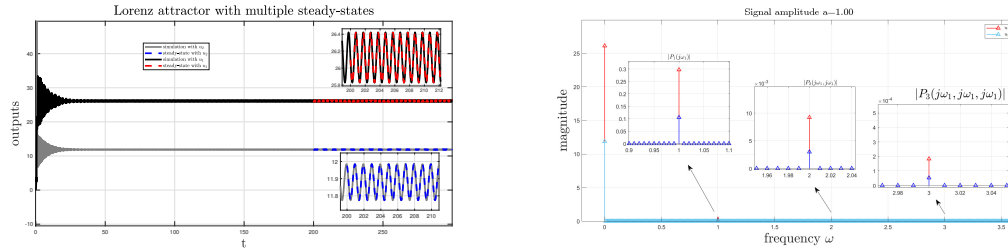


Figure 4: Multiple steady-states and corresponding power spectrum. More details in the [table 2](#).

Data	DC	$H_1(j\omega_1)$	$H_2(j\omega_1, j\omega_2)$	$H_3(j\omega_1, j\omega_2, j\omega_3)$
$u_1(t)$	11.8819	$-0.0148 + 0.2971i$	$-0.00687 - 0.00614i$	$1.74e - 4 - 5.82e - 5i$
$u_2(t)$	26.1181	$0.09303 + 0.05011i$	$-3.0e - 4 - 3.0e - 3i$	$6.0e - 6 + 5.3e - 5i$

Table 2: In this table, and for each system (blue, red), the Fourier spectrum (magnitude, phase) P provides the following measurements (complex inputs): $H_1(j\omega_1) = \frac{P_1(j\omega_1)}{a}$, $H_2(j\omega_1, j\omega_2) = \frac{P_2(j\omega_1, j\omega_2)}{a^2}$, $H_3(j\omega_1, j\omega_2, j\omega_3) = \frac{P_3(j\omega_1, j\omega_2, j\omega_3)}{a^3}$. For each system, the DC term, e.g., (60), can be computed from the non-periodic value $P(0)$ in the power spectrum. This can be generalized for multi-harmonic real signals (kernel separation) and in the X -parameter machinery [52] that deals with harmonic distortion.

function that can interpret the measurements in [table 2](#) has to do with the corresponding linear operator e.g., $\tilde{\mathbf{A}}_q = \mathbf{A} + 2\mathbf{Q}(\mathbf{x}_e^{(q)} \otimes \mathbf{I})$, $q = 1, 2$ and for each equilibrium respectively. For instance, using the equilibrium $\mathbf{x}_e^{(1)}$, we compute $\tilde{\mathbf{A}}_1 = \mathbf{A} + 2\mathbf{Q}(\mathbf{x}_e^{(1)} \otimes \mathbf{I})$. The 1st transfer function H_1 (for the equilibrium $\mathbf{x}_e^{(1)}$) yields the following value at frequency $\omega_1 = 2\pi$: $H_1(j\omega_1) = \mathbf{C}(j\omega_1 \mathbf{I} - \tilde{\mathbf{A}}_1)^{-1} \mathbf{B} = -0.0148 + 0.2971i$ which explains the measurements in the 1st row of [table 2](#), and similarly, the higher kernels explain the rest. Similar results can be obtained for the 2nd input- u_2 and for the higher kernels. One way to distinguish different operational points (steady-states) among different equilibrium points is through the non-periodic term. For instance, when the Lorenz system is concerned with $\rho = 20 > 1$, we measure two different local quadratic systems that can be recognised from the two different DC terms in [fig. 4](#). Thus, the two different quadratic systems (43) can be identified and the dynamics of the local coordinate system can be explained, with the respective equilibrium point as the origin. To discover the original model that has been bifurcated, we need to align the invariant operators to the same coordinates. Starting with a random seed for the Newton method e.g., $\mathbf{T}_0 \sim \mathcal{N}(\boldsymbol{\mu}, \boldsymbol{\sigma})$, and applying

⁵With complex inputs, e.g., $u(t) : \mathbb{R}_+ \rightarrow \mathbb{C}$, indexing harmonics and estimating kernels are straightforward tasks compared to the real input case e.g., $u(t) : \mathbb{R}_+ \rightarrow \mathbb{R}$, where additional operations s.a. kernel separation with amplitude shifting, should be addressed [16, 37, 52].

algorithm 3, we have the following convergence in fig. 5 to the solution:

$$\mathbf{T}^{-1} = \begin{bmatrix} -0.003881 & -1.308 & -4.584 \\ -0.2823 & -0.8908 & -1.193 \\ -0.2035 & 0.6238 & 1.575 \end{bmatrix} \quad (70)$$

Now, the two quadratic systems have been aligned with the transformation \mathbf{T} and the equilibrium points can be computed by solving (59) coupled with the information from the DC-terms (60) together with the enforcement of the operators $\hat{\mathbf{L}}, \check{\mathbf{L}}$ at the equilibrium points to be zero as analyzed in (62). Finally, by solving the above-coupled systems, we have the following results:

$$\boldsymbol{\lambda} = \begin{bmatrix} +20.45 \\ -58.29 \end{bmatrix}, \quad \hat{\mathbf{x}}_e^{(1)} = \begin{bmatrix} 61.15 \\ 26.78 \\ 11.24 \end{bmatrix}, \quad \check{\mathbf{x}}_e^{(2)} = \begin{bmatrix} -16.28 \\ -45.49 \\ 11.39 \end{bmatrix}. \quad (71)$$

Having found the equilibrium points, we can derive the original linear operator from

$$\mathbf{A}_1 = \hat{\mathbf{A}}_1 - 2\hat{\mathbf{Q}}_1 \left(\hat{\mathbf{x}}_e^{(1)} \otimes \mathbf{I} \right) = \begin{bmatrix} -7.873 & 7.255 & 66.07 \\ 3.056 & -7.245 & -48.22 \\ 1.602 & -1.405 & 1.451 \end{bmatrix}. \quad (72)$$

This linear operator \mathbf{A}_1 has the same eigenvalues with the original linear operator from the Lorenz system $\rho = 20$, $\text{eig}(\mathbf{A}_1) = \text{eig}(\mathbf{A}) = (-20.34 \quad -2.667 \quad 9.341)$. With the proposed method we were able to identify the original Lorenz system with the unstable linear operator. After transforming the operators $(\mathbf{A}_1, \mathbf{Q}_1, \mathbf{B}_1, \mathbf{C}_1)$ to the original coordinates appendix A, the two systems; original (65) and identified are exactly the same fig. 5(right).

Case 3 - $\rho = 28$. Since for this parameter range (when $\rho > 24.74$), the dynamics are chaotic with the state evolution bifurcating from one equilibrium to the other without requiring additional energy, a steady state cannot be achieved, and measurements cannot be obtained for the higher kernels. Identifying such systems is not within the scope of this study. Generally, for any identification method, the operators can be identified to a finite numerical precision (e.g., IEEE machine precision $\epsilon \approx 2.22e-16$). Since this is already an approximation with a non-zero numerical error, this slight numerical discrepancy will not allow any safe prediction of such a sensitive system as the (deterministic) chaotic Lorenz attractor.

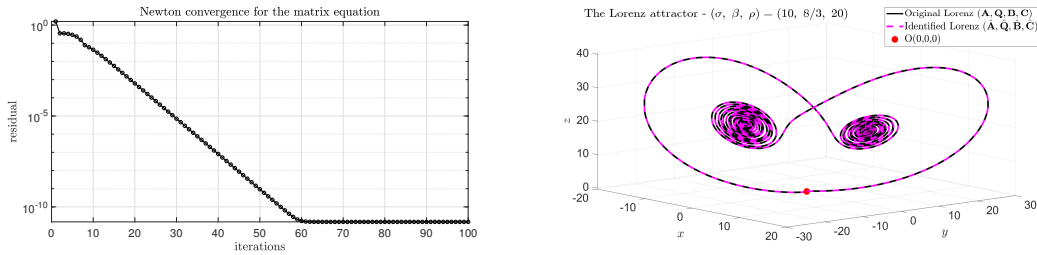


Figure 5: **Left:** Convergence of the Newton scheme in algorithm 3. **Right:** The original Lorenz system is identified with the two nontrivial equilibrium points. Here is the comparison between the original system and the identified one. The constructed state space evolution for both systems and at the same coordinates remains the same with zero numerical error.

3.2. Reduction of the Burgers' viscous equation

In this example, we want to illustrate the proposed method in a larger-scale example. The aim is to construct robust surrogate models of a reduced order directly from physical measurements (i.e., samples of the symmetric GFRFs obtained from time-domain simulations) that provide efficient approximations. A detailed description of the model under consideration can be found in [4]. We keep the same model set-up with a different viscosity parameter ν and observation space. Here, we consider as an output the velocity of the last tip of the flow $y(t) = x_{n+1}(t)$. Thus, the vector \mathbf{C} contains

everywhere zeros except from the last entry, which is 1. As illustrated in the study [4], the Loewner models for small viscosity coefficients ν may produce unstable results. As the current study relies on the Volterra series representation, analysis of the convergence with arbitrary viscosity and input amplitude remains an open issue. Hence, we illustrate a more conservative case with higher viscosity in what follows. We use the problem data $\nu = 0.5$, $\sigma_0 = 0$, $\sigma_1 = 0.1$ representing the same physical quantities as in [4]. The full order model (FOM) is the linear finite element semi-discretization with $n = 257$. The semi-discretized system can result in (11) after inverting with the well-conditioned mass matrix \mathbf{E} . The system (11) solution is approximated with the Runge-Kutta multi-step integration method with a uniform time-discretization step $dt = 1/1000$. In the simulation bellow, we use $u_0(t) = 0.1e^{-0.2t}\text{sawtooth}(t) + 0.1\sin(4\pi t)$, and $u_1 \equiv 0$. Similarly, as in the Lorenz example, we take the following measurements:

- 100 logarithmic distributed measurements from the interval $[10^{-3}, 10^1]$,
- 400 logarithmic distributed measurements from the square grid $[10^{-3}, 10^1]^2$,
- 216 logarithmic distributed measurements from the cubic grid $[10^{-3}, 10^1]^3$.

In fig. 7 (left), the singular value decay of the Loewner framework is presented. Thus, we choose the minimal linear order $r = 6$ with the first normalized truncated singular value of magnitude $\sigma_7/\sigma_1 = 5.10418 \cdot 1e - 10$. The recovery of the 1st GFRFs H_1 that results from the FOM with dimension $n = 257$ is compared with the reduced \hat{H}_1 of dimension $r = 6$ in fig. 7(left). Towards the estimation of the quadratic operator from the measurements of the 2nd GFRF H_2 (FOM) and after solving (30) with a threshold $\eta = 1e - 8$, we get the quadratic operator $\mathbf{Q}_s \in \mathbb{R}^{6 \times 6^2}$. The hyper-parameter is tested for balancing the error with the norm of $\|\mathbf{Q}\|$ in a classical regularization sense. There are different ways to find the optimal regularization parameter η , e.g., Tikhonov regularization, L-curve that work similarly as with the thresholding SVD. Moreover, the choice of η affects the length of the null space. In particular, out of $r^3 = 6^3 = 216$ degrees of freedom (DoF) and after enforcing the symmetries of the quadratic operator, the maximum rank could be $\text{rank} = 141 < 216$ when η is close to machine precision. Therefore, inverting with threshold $\eta = 1e - 8$, the rank is 128 and the resulting null space has length $216 - 128 = 88$. These extra 88 free parameters will be estimated so as to interpolate the 3rd GFRF as well. The fit performance between the 2nd level GFRFs from both FOM and ROM systems is illustrated in fig. 6(left). At this level, we estimate the quadratic operator

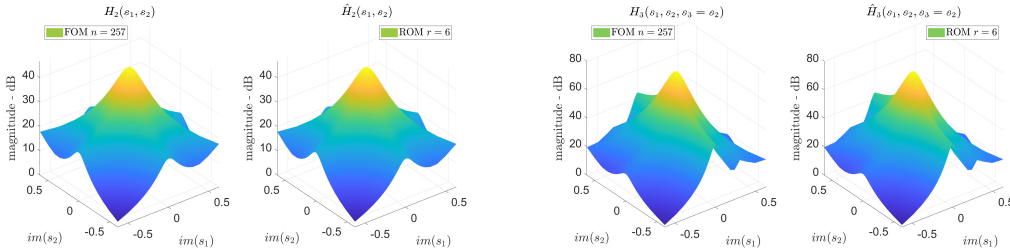


Figure 6: Comparison between the FOM and ROM on the left, for the 2nd level kernels $\|\mathbf{H}_2(\mathbf{s}_1, \mathbf{s}_2) - \hat{\mathbf{H}}_2(\mathbf{s}_1, \mathbf{s}_2)\| = 3.1577e - 05$, and on the right, for the 3rd level kernels. The error over the 2D plain-domain after fixing the 3rd dimension as $\mathbf{s}_2 = \mathbf{s}_3$ is $\|\mathbf{H}_3(\mathbf{s}_1, \mathbf{s}_2, \mathbf{s}_2 = \mathbf{s}_3) - \hat{\mathbf{H}}_3(\mathbf{s}_1, \mathbf{s}_2, \mathbf{s}_2 = \mathbf{s}_3)\| = 5.0353e - 05$.

denoted \mathbf{Q}_s with information coming from the first two kernels H_1, H_2 . Using the parameterization with λ_i , $i = 1, \dots, 88$ from (31), we enforce interpolation with the 3rd GFRF H_3 so to estimate the remaining $m = 88$ parameters. Forming the data matrices in algorithm 1, with hyper-parameter tuning as $\eta = 1e - 9$, $\gamma_0 = 1e - 5$, the residue of the Newton iterations stagnates to $2.2478e - 06$. In fig. 6(right) comparison between the 3rd level kernels FOM($n = 257$) and ROM($r = 6$) is depicted.

Kernels & frequencies	Evaluation at $(s_1, s_2, s_3) = (1i, 2i, 3i)$	Interpolation with the FOM
FOM $H_2(s_1, s_2)$	$-0.20829 + 0.13846i$	theoretical value
$\hat{H}_2(s_1, s_2, \mathbf{Q}_r)$	$-0.20829 + 0.13846i$	✓
$\hat{H}_2(s_1, s_2, \mathbf{Q}_s)$	$-0.20829 + 0.13846i$	✓
FOM $H_3(s_1, s_2, s_3)$	$0.042016 + 0.027069i$	theoretical value
$\hat{H}_3(s_1, s_2, s_3, \mathbf{Q}_r, \mathbf{Q}_r)$	$0.042015 + 0.027069i$	✓
$\hat{H}_3(s_1, s_2, s_3, \mathbf{Q}_s, \mathbf{Q}_s)$	$0.031301 + 0.00015172i$	×

Table 3: Symmetric Volterra kernel interpolation at a random point. The updated \mathbf{Q}_r from the three kernels enforces interpolation to the 3rd kernel without ruining the interpolation on the 2nd kernel. As a result, the overall performance has improved significantly [fig. 7\(right\)](#).

Finally, in [fig. 7](#), both systems FOM($n = 257$) and ROM($r = 6$) are compared under a nontrivial input and for an extended simulation that covers all the dynamic evolution starting from a hard transient up to the steady-state profile. By considering more measurements from higher-order kernels, the fitting performance improves significantly (for the complete time interval of the simulation). The proposed method achieves approximate interpolation to all the measurement data sets and the accuracy performance is improved when using the three kernels [fig. 7\(right\)](#). The updated quadratic operator $\hat{\mathbf{Q}}$ of dimension 6×6^2 interpolates approximately the 3rd kernel. To illustrate this result, in [table 3](#), we choose a random point in the three-dimensional frequency space, and we test the interpolation error for both estimations of the quadratic operator; firstly, from the two kernels as \mathbf{Q}_s ; secondly, from the three kernels as \mathbf{Q}_r .

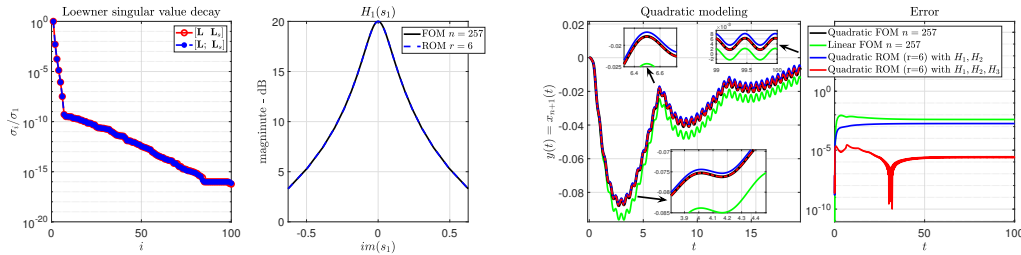


Figure 7: From left to right, the singular value decay of the Loewner matrix. Comparison between the FOM and ROM 1st level kernels with error $\|\mathbf{H}_1(s_1) - \hat{\mathbf{H}}_1(s_1)\| = 8.9852e - 09$. Reduction of a percentage level 98% has been achieved with the error between the FOM($n = 257$) and ROM($r = 6$) to be $\|\hat{y}(t) - y(t)\| \approx 1e - 5$.

4. Discussion and concluding remarks

In this study, we were concerned with identifying or constructing quadratic state-space models from i/o time domain data. Such models can be obtained from the first principles, e.g., Newtonian dynamics that result in second-order $\ddot{\mathbf{x}}(t) \in \mathbb{R}^n$, and after transforming equivalently to first-order $\dot{\mathbf{x}}(t) \in \mathbb{R}^{2n}$, we result in systems with ODEs of a specific nonlinear degree. For instance, dynamical systems that belong to the class of quadratic control are; Navier Stokes, Burgers' equation, Lorenz attractor, etc. Using the symmetric generalized frequency Volterra kernels that can be estimated from a physical system under input-output harmonic excitation, the proposed method identifies/constructs quadratic models. By having estimations of a finite set out of the infinite Volterra kernels, and after enforcing interpolation, e.g., to the first three (H_1, H_2, H_3), the resulting quadratic system inherits a Volterra series that interpolates the original one to a specific set of chosen frequency points for the first kernels

and approximates the rest of the infinite terms that eventually decay to negligible dynamics. The proposed method is not limited to systems bifurcating into different equilibrium points. The steady-state measurements explain the local behavior of the phenomenon without ensuring that the actual dynamics are not described from a global model that bifurcates to different equilibrium points. Therefore, we have illustrated this phenomenon from the forced Lorenz attractor model with parameters that produce this effect. With the proposed method, we identified the global model of the Lorenz attractor from i/o time domain data and with parameters ($\sigma = 10$, $\beta = 8/3$, $\rho = 20$), after taking care of the invariant information that carries along the different equilibrium points. The proposed method has been tested w.r.t. the reduction performance for a larger-scale example (the Burgers' equation), and a quadratic surrogate model has been constructed of order $r = 6$ that achieved 98% reduction and accuracy close to 5 digits. For systems that involve different nonlinear dynamics, such as classical oscillators, e.g., Duffing, Van der Pol, etc., the same analysis can be derived for polynomial state-space systems to a specific nonlinear degree s.a. cubic order, i.e., $\mathbf{x} \otimes \mathbf{x} \otimes \mathbf{x}$ that physically can explain nonlinear stiffness and damping. Lifting strategies for equivalently representing nonlinear systems with analytical nonlinearities to the quadratic form are left for future research endeavors as the main difficulty for non-intrusive methods such as the one presented here is to deal with a "partially missing" linear operator \mathbf{A} . Therefore, we aim to analyze such phenomena in the future, i.e., for which the resolvent $\Phi(s) = (s\mathbf{I} - \mathbf{A})^{-1}$ contains a sparse linear operator \mathbf{A} , that may contain many zero diagonal blocks (due to, e.g., applying lifting approaches). Although the tools used in this study are robust to noise (such as most spectral transforms), more involved analysis of the impact of the noise is left for future studies. Moreover, we plan to involve machine learning techniques that can be advantageous to methods such as the proposed one due to their power to learn nonlinear i/o maps (universal approximation theorem). For instance, when solely one input-output sequence of measurements is accessible (and not many such sequences), a neural network (NN) can be used as a surrogate black box model for transferring the whole measurement process to more efficient, cheap simulations. Finally, by connecting data and computational science tools, e.g., NNs, with the proposed method, will contribute to an increase in interpretability for ML tools. More precisely, by constructing interpretable state-space dynamic models, for which the analysis has matured over many decades, ad-hoc engineering practices will become more reliable.

A. Coordinates

Dynamical systems that form an equivalent modulo can be aligned by means of a similarity transform $\Psi \in \mathbb{R}^{n \times n}$ as:

$$\begin{aligned} \Phi_1 &= [C_1 \mathbf{A}_1 \quad C_1 \mathbf{A}_1^2 \quad \cdots \quad C_1 \mathbf{A}_1^n], \quad \Phi_2 = [C_2 \mathbf{A}_2 \quad C_2 \mathbf{A}_2^2 \quad \cdots \quad C_2 \mathbf{A}_2^n], \\ \Psi &= \Phi_2^{-1} \Phi_1, \quad \text{and for the operators of the quadratic system holds:} \\ (\mathbf{A}_2, \mathbf{Q}_2, \mathbf{B}_2, \mathbf{C}_2) &= (\Psi^{-1} \mathbf{A}_1 \Psi, \Psi^{-1} \mathbf{Q}_1 (\Psi \otimes \Psi), \Psi^{-1} \mathbf{B}_1, \mathbf{C}_1 \Psi). \end{aligned} \tag{73}$$

Acknowledgments

The first author would like to acknowledge that this work was supported mainly by the Max Planck Institute in Magdeburg during his Ph.D. project.

References

- [1] B. D. O. Anderson and A. C. Antoulas, Rational interpolation and state-variable realizations, *Linear Algebra and Its Applications*, 137/138 (1990), pp. 479–509.
- [2] A. C. Antoulas, Approximation of large-scale dynamical systems, SIAM, Philadelphia, 2005.

-
- [3] A. C. Antoulas, C. A. Beattie, and S. Gugercin, Interpolatory Methods for Model Reduction, SIAM, Philadelphia, 2020.
- [4] A. C. Antoulas, I. V. Gosea, and M. Heinkenschloss, On the Loewner framework for model reduction of Burgers' equation, in Active Flow and Combustion Control, R. King, ed., Springer, Cham, Switzerland, 2019, pp. 255–270.
- [5] A. C. Antoulas, I. V. Gosea, and A. C. Ionita, Model reduction of bilinear systems in the Loewner framework, SIAM Journal on Scientific Computing, 38(5) (2016), pp. B889–B916.
- [6] A. C. Antoulas, S. Lefteriu, and A. C. Ionita, A tutorial introduction to the Loewner Framework for Model Reduction, Model Reduction and Approximation for Complex Systems, Edited by P. Benner, A. Cohen, M. Ohlberger, and K. Willcox, Series: Computational Science & Engineering, <https://doi.org/10.1137/1.9781611974829>, SIAM, 2017, pp. 335–376.
- [7] U. Baur, P. Benner, and L. Feng, Model order reduction for linear and nonlinear systems: a system-theoretic perspective, Archives of Computational Methods in Engineering, 21 (2014), pp. 331–358.
- [8] P. Benner and L. Feng, Model order reduction based on moment-matching, in Model Order Reduction: Volume 1: System-and Data-Driven Methods and Algorithms, De Gruyter, 2021, pp. 57–96.
- [9] P. Benner and P. Goyal, Interpolation-based model order reduction for polynomial systems, SIAM Journal on Scientific Computing, 43 (2021), pp. A84–A108, <https://doi.org/10.1137/19M1259171>.
- [10] P. Benner, P. Goyal, B. Kramer, B. Peherstorfer, and K. Willcox, Operator inference for non-intrusive model reduction of systems with non-polynomial nonlinear terms, CompMethApp-MechEng, 372 (2020), p. 113433, <https://doi.org/10.1016/j.cma.2020.113433>.
- [11] P. Benner, S. Grivet-Talocia, A. Quarteroni, G. Rozza, W. Schilders, and L. M. Silveira, eds., Model Order Reduction Volume 2: Snapshot-Based Methods and Algorithms, De Gruyter, Berlin, Boston, 2020, <https://doi.org/doi:10.1515/9783110671490>.
- [12] P. Benner, S. Grivet-Talocia, A. Quarteroni, G. Rozza, W. Schilders, and L. M. Silveira, eds., Model Order Reduction Volume 3: Applications, De Gruyter, Berlin, Boston, 2020, <https://doi.org/doi:10.1515/9783110499001>.
- [13] P. Benner, S. Grivet-Talocia, A. Quarteroni, G. Rozza, W. Schilders, and L. M. Silveira, eds., Model Order Reduction Volume 1: System- and Data-Driven Methods and Algorithms, De Gruyter, Berlin, Boston, 2021, <https://doi.org/doi:10.1515/9783110498967>.
- [14] S. A. Billings, Nonlinear System Identification: NARMAX Methods in the Time, Frequency, and Spatio-Temporal Domains, Wiley, 2013.
- [15] S. Boyd and L. S. Chua, Fading memory and the problem of approximating nonlinear operators with volterra series, IEEE Transactions on Circuits and Systems, 30 (1985), pp. 1150–1161.
- [16] S. Boyd, Y. shing Tang, and L. O. Chua, Measuring Volterra kernels, in IEEE transactions on circuits and systems, 1983.
- [17] T. Breiten and T. Stykel, 2 balancing-related model reduction methods, System-and Data-Driven Methods and Algorithms, (2021), pp. 15–56.
- [18] S. Brunton and J. Kutz, Data-Driven Science and Engineering: Machine Learning, Dynamical Systems, and Control, Cambridge University Press, 2022, <https://books.google.de/books?id=rxNkEAAAQBAJ>.

-
- [19] S. L. Brunton, J. L. Proctor, and J. N. Kutz, Discovering governing equations from data by sparse identification of nonlinear dynamical systems, *Proceedings of the National Academy of Sciences*, 113 (2016), pp. 3932–3937, <https://doi.org/10.1073/pnas.1517384113>.
- [20] H. Chen and J. Maciejowski, Subspace identification method for combined deterministic-stochastic bilinear systems, *IFAC Proceedings Volumes*, 33 (2000), pp. 229–234, [https://doi.org/https://doi.org/10.1016/S1474-6670\(17\)39755-0](https://doi.org/https://doi.org/10.1016/S1474-6670(17)39755-0). 12th IFAC Symposium on System Identification (SYSID 2000), Santa Barbara, CA, USA, 21-23 June 2000.
- [21] S. Chen and S. A. Billings, Representations of non-linear systems: the narmax model, *International Journal of Control*, 49 (1989), pp. 1013–1032, <https://doi.org/10.1080/00207178908559683>.
- [22] W. Favoreel, B. De Moor, and P. Van Overschee, Subspace identification of bilinear systems subject to white inputs, *IEEE Transactions on Automatic Control*, 44 (1999), pp. 1157–1165, <https://doi.org/10.1109/9.769370>.
- [23] I. V. Gosea, Exact and inexact lifting transformations of nonlinear dynamical systems: Transfer functions, equivalence, and complexity reduction, *Applied Sciences*, 12 (2022), <https://doi.org/10.3390/app12052333>.
- [24] I. V. Gosea and A. C. Antoulas, Model reduction of linear and nonlinear systems in the loewner framework: A summary, in *2015 European Control Conference (ECC)*, 2015, pp. 345–349, <https://doi.org/10.1109/ECC.2015.7330568>.
- [25] I. V. Gosea and A. C. Antoulas, Data-driven model order reduction of quadratic-bilinear systems, *Numerical Linear Algebra with Applications*, 25 (2018), p. e2200, <https://doi.org/10.1002/nla.2200>.
- [26] I. V. Gosea, D. S. Karachalios, and A. C. Antoulas, Learning reduced-order models of quadratic dynamical systems from input-output data, in *2021 European Control Conference (ECC)*, IEEE, 2021, pp. 1426–1431.
- [27] I. V. Gosea, M. Petreczky, and A. C. Antoulas, Data-driven model order reduction of linear switched systems in the loewner framework, *SIAM Journal on Scientific Computing*, 40 (2018), pp. B572–B610, <https://doi.org/10.1137/17M1120233>.
- [28] I. V. Gosea, M. Petreczky, and A. C. Antoulas, Reduced-order modeling of LPV systems in the Loewner framework, in *2021 60th IEEE Conference on Decision and Control (CDC)*, 2021, pp. 3299–3305, <https://doi.org/10.1109/CDC45484.2021.9683742>.
- [29] C. Gu, A projection-based nonlinear model order reduction approach using quadratic-linear representation of nonlinear systems, *IEEE Transactions on Computer-Aided Design of Integrated Circuits and Systems*, 30 (2011), pp. 1307–1320.
- [30] B. Gustavsen and A. Semlyen, Rational approximation of frequency domain responses by vector fitting, *IEEE Transactions on Power Delivery*, 14 (1999), pp. 1052–1061, <https://doi.org/10.1109/61.772353>.
- [31] S. M. Hirsch, K. D. Harris, J. N. Kutz, and B. W. Brunton, Centering data improves the dynamic mode decomposition, *SIAMAppDynSys*, 19 (2020), pp. 1920–1955, <https://doi.org/10.1137/19M1289881>.
- [32] B. L. Ho and R. E. Kalman, Effective construction of linear state-variable models from input/output functions, at - *Automatisierungstechnik*, 14 (1966), pp. 545–548, <https://doi.org/10.1524/auto.1966.14.112.545>.

- [33] A. Isidori, Direct construction of minimal bilinear realizations from nonlinear input-output maps, IEEE Transactions on Automatic Control, 18 (1973), pp. 626–631, <https://doi.org/10.1109/TAC.1973.1100424>.
- [34] J.-N. Juang and R. S. Pappa, An eigensystem realization algorithm for modal parameter identification and model reduction, Journal of Guidance, Control, and Dynamics, 8 (1985), pp. 620–627, <https://doi.org/10.2514/3.20031>.
- [35] D. S. Karachalios, I. V. Gosea, and A. C. Antoulas, A bilinear identification-modeling framework from time domain data, PAMM, 19 (2019), p. e201900246, <https://doi.org/10.1002/pamm.201900246>.
- [36] D. S. Karachalios, I. V. Gosea, and A. C. Antoulas, The Loewner framework for system identification and reduction, De Gruyter, Berlin, Boston, 2021, pp. 181–228, <https://doi.org/doi:10.1515/9783110498967-006>.
- [37] D. S. Karachalios, I. V. Gosea, and A. C. Antoulas, On bilinear time-domain identification and reduction in the Loewner framework, in Model Reduction of Complex Dynamical Systems, vol. 171 of International Series of Numerical Mathematics, Birkhäuser, Cham, 2021, pp. 3–30, https://doi.org/10.1007/978-3-030-72983-7_1.
- [38] D. S. Karachalios, I. V. Gosea, and A. C. Antoulas, A framework for fitting quadratic-bilinear systems with applications to models of electrical circuits, IFAC-PapersOnLine, 55 (2022), pp. 7–12, <https://doi.org/https://doi.org/10.1016/j.ifacol.2022.09.064>. 10th Vienna International Conference on Mathematical Modelling MATHMOD 2022.
- [39] P. Khodabakhshi and K. E. Willcox, Non-intrusive data-driven model reduction for differential–algebraic equations derived from lifting transformations, Computer Methods in Applied Mechanics and Engineering, 389 (2022), p. 114296, <https://doi.org/https://doi.org/10.1016/j.cma.2021.114296>.
- [40] D. Kleinman, On an iterative technique for Riccati equation computations, IEEE Transactions on Automatic Control, 13 (1968), pp. 114–115, <https://doi.org/10.1109/TAC.1968.1098829>.
- [41] K. K. Lin and F. Lu, Data-driven model reduction, Wiener projections, and the Koopman-Mori-Zwanzig formalism, Journal of Computational Physics, 424 (2021), p. 109864, <https://doi.org/https://doi.org/10.1016/j.jcp.2020.109864>.
- [42] P. Lopes dos Santos, J. A. Ramos, and J. L. Martins de Carvalho, Identification of bilinear systems with white noise inputs: An iterative deterministic-stochastic subspace approach, IEEE Transactions on Control Systems Technology, 17 (2009), pp. 1145–1153, <https://doi.org/10.1109/TCST.2008.2002041>.
- [43] E. N. Lorenz, Deterministic nonperiodic flow, Journal of Atmospheric Sciences, 20 (1963), pp. 130–141, [https://doi.org/10.1175/1520-0469\(1963\)020<0130:DNF>2.0.CO;2](https://doi.org/10.1175/1520-0469(1963)020<0130:DNF>2.0.CO;2).
- [44] A. J. Mayo and A. C. Antoulas, A framework for the generalized realization problem, Linear Algebra and Its Applications, 426 (2007), pp. 634–662.
- [45] Y. Nakatsukasa, O. Sète, and L. N. Trefethen, The aaa algorithm for rational approximation, SIAM Journal on Scientific Computing, 40 (2018), pp. A1494–A1522, <https://doi.org/10.1137/16M1106122>.
- [46] B. Peherstorfer, S. Gugercin, and K. Willcox, Data-driven reduced model construction with time-domain loewner models, SIAM Journal on Scientific Computing, 39 (2017), pp. A2152–A2178, <https://doi.org/10.1137/16M1094750>.

-
- [47] B. Peherstorfer and K. Willcox, Data-driven operator inference for nonintrusive projection-based model reduction, *Computer Methods in Applied Mechanics and Engineering*, 306 (2016), pp. 196–215, <https://doi.org/10.1016/j.cma.2016.03.025>.
- [48] J. L. Proctor, S. L. Brunton, and J. N. Kutz, Dynamic mode decomposition with control, *SIAM Journal on Applied Dynamical Systems*, 15 (2016), pp. 142–161, <https://doi.org/10.1137/15M1013857>.
- [49] W. J. Rugh, Nonlinear system theory - The Volterra/Wiener Approach, The Johns Hopkins University Press, 1981.
- [50] P. J. SCHMID, Dynamic mode decomposition of numerical and experimental data, *Journal of Fluid Mechanics*, 656 (2010), p. 5–28, <https://doi.org/10.1017/S0022112010001217>.
- [51] R. Toth, H. S. Abbas, and H. Werner, On the state-space realization of lpv input-output models: Practical approaches, *IEEE Transactions on Control Systems Technology*, 20 (2012), pp. 139–153, <https://doi.org/10.1109/TCST.2011.2109040>.
- [52] Verspecht and D. Root, Polyharmonic distortion modeling, *IEEE Microwave Magazine*, 7 (2006), pp. 44–57, <https://doi.org/10.1109/MMW.2006.1638289>.
- [53] J. Weiss, A tutorial on the proper orthogonal decomposition, in 2019 AIAA Aviation Forum, American Institute of Aeronautics and Astronautics, 2019, pp. AIAA 2019–3333, <https://depositonce.tu-berlin.de/handle/11303/9456>.
- [54] X. Y. Z. Xiong, L. J. Jiang, J. E. Schutt-Ainé, and W. C. Chew, Volterra series-based time-domain macromodeling of nonlinear circuits, *IEEE Transactions on Components, Packaging and Manufacturing Technology*, 7 (2017), pp. 39–49, <https://doi.org/10.1109/TCPMT.2016.2627601>.